JBC RESEARCH ARTICLE

NPC1 plays a role in the trafficking of specific cargo to melanosomes

Received for publication, March 21, 2023, and in revised form, June 20, 2023 Published, Papers in Press, July 7, 2023,
https://doi.org/10.1016/j.jbc.2023.105024

Alina Adriana Rus[1], Ioana V. Militaru[1], Ioana Popa[1], Cristian V. A. Munteanu[2], Livia Elena Sima[1], Nick Platt[3], Frances M. Platt[3], and Ștefana M. Petrescu[1,*]

From the [1]Department of Molecular Cell Biology, and [2]Department of Bioinformatics and Structural Biochemistry, Institute of Biochemistry, Bucharest, Romania; [3]Department of Pharmacology, University of Oxford, Oxford, UK

Reviewed by members of the JBC Editorial Board. Edited by Phyllis Hanson

Niemann–Pick type C1 (NPC1) protein is a multimembrane spanning protein of the lysosome limiting membrane that facilitates intracellular cholesterol and sphingolipid transport. Loss-of-function mutations in the NPC1 protein cause Niemann–Pick disease type C1, a lysosomal storage disorder characterized by the accumulation of cholesterol and sphingolipids within lysosomes. To investigate whether the NPC1 protein could also play a role in the maturation of the endo-lysosomal pathway, here, we have investigated its role in a lysosome-related organelle, the melanosome. Using a NPC1-KO melanoma cell model, we found that the cellular phenotype of Niemann–Pick disease type C1 is associated with a decreased pigmentation accompanied by low expression of the melanogenic enzyme tyrosinase. We propose that the defective processing and localization of tyrosinase, occurring in the absence of NPC1, is a major determinant of the pigmentation impairment in NPC1-KO cells. Along with tyrosinase, two other pigmentation genes, tyrosinase-related protein 1 and Dopachrome-tautomerase have lower protein levels in NPC1 deficient cells. In contrast with the decrease in pigmentation-related protein expression, we also found a significant intracellular accumulation of mature PMEL17, the structural protein of melanosomes. As opposed to the normal dendritic localization of melanosomes, the disruption of melanosome matrix generation in NPC1 deficient cells causes an accumulation of immature melanosomes adjacent to the plasma membrane. Together with the melanosomal localization of NPC1 in WT cells, these findings suggest that NPC1 is directly involved in tyrosinase transport from the *trans*-Golgi network to melanosomes and melanosome maturation, indicating a novel function for NPC1.

The Niemann–Pick type C1 (NPC1) gene encodes a multipass membrane glycoprotein found in the limiting membrane of late endosomes/lysosomes. Before reaching the endolysosomal compartment, the protein is synthesized in the endoplasmic reticulum (ER) and transported to the Golgi and from the *trans*-Golgi network (TGN) to late endosomes/lysosomes (1). Loss-of-function mutations in the NPC1 gene are responsible for the Niemann–Pick disease type C1 (NPC) characterized by the accumulation of glycosphingolipids, sphingomyelin, sphingoid bases, and cholesterol in late endosomes/lysosomes (2, 3). Although NPC1 function has not been precisely elucidated, it has been proposed that it coordinates cholesterol efflux from lysosome toward other cell compartments such as the ER or plasma membrane (4–6). It is reasonable to assume that specialized lysosome-related organelles (LRO) with distinct functions occurring in specialized cells, such as Weibel–Palade bodies in endothelial cells, dense granules in platelets, lamellar bodies in lung cells, and melanosomes in pigment cells could show similar malfunction as conventional lysosomes (7, 8). Indeed, loss of NPC1 results in natural killer cells and platelet functional defects that have been associated with reduced acidic store Ca^{2+} levels affecting the LRO secretion (9, 10). Based on these findings, we hypothesized that the biogenesis of another specialized LRO, the melanosome, required for the pigmentation process occurring in melanocytes, may also be affected by NPC1 loss.

Melanosomes acquire the melanogenic proteins delivered from specific membrane sites of the endolysosomal pathway and other cellular compartments, maturing into independent, pigment laden LRO (11, 12). A central role in melanosome biogenesis is attributed also to a premelanosome protein (PMEL17), a structural protein sorted from the intraluminal vesicles of an early endosomal compartment, to initiate the building up of the melanosomal fibrillar matrix. Following its passage through the Golgi complex, PMEL17 is cleaved by different convertases en-route to the plasma membrane and further in endosomes. The complex sequence of cleavage events finally leads to mature PMEL17 that forms the amyloid-like fibrils of melanosomes onto which melanin is deposited (13). The melanin biosynthetic process takes place in melanosomes, where tyrosinase (TYR), tyrosinase-related protein 1 (TYRP)-1, and dopachrome-tautomerase (DCT) play a major role in the synthesis of melanin from L-tyrosine. TYR is central in the pathway, catalyzing the rate-limiting step of melanogenesis and in its absence melanin is not synthesized, as seen in patients with oculocutaneous albinism type IA (14–16). As such, a defective processing of TYR, mutations in TYR gene, or an altered transport to melanosomes can lead to pigmentation defects. TYR is a glycoprotein whose folding and maturation are highly

* For correspondence: Ștefana M. Petrescu, stefana.petrescu@biochim.ro.

dependent on the N-glycosylation process that starts within the ER (17–19). Misfolded TYR mutants are recognized by EDEM1 and removed from the ER by ER-associated degradation, targeting for proteasomal degradation (20). Folded TYR molecules are exported from the ER to the Golgi, where they undergo complex N-glycosylation processing. TYR is transported to melanosomes from the Golgi *via* an endocytic pathway, although it remains unclear how it is diverted from lysosomes (21–23). To accomplish the pigmentation process, the melanin pigment is deposited on the fibril melanosomal matrix generated by PMEL17 and contributes to the maturation of melanosomes, the pigmented organelles of the skin, hair, and eyes (13).

Understanding the role of NPC1 in the biogenesis of a specialized LRO organelle could shed new light on identifying specific pathways used in specialized cells for diverting the cargo destined for LRO from lysosomal degradation. In the current study, we investigated the influence of NPC1 protein silencing on melanogenesis. We found that in melanoma cells lacking NPC1, the perturbance of the endocytic pathway occurs and pigmentation was inhibited. Furthermore, we demonstrate that the impairment of TYR expression, processing, and intracellular localization are contributory causes of this lack of pigmentation. In addition, NPC1 deficient melanoma cells exhibited elevated levels of the mature amyloidogenic form of PMEL17. This study underscores a new role for the NPC1 protein, underlying its essential role in melanogenesis process and LRO biogenesis.

Results

Cell model for studying the influence of NPC1 protein deficiency on pigmentation process

In order to study the impact of NPC1 deficiency on cell pigmentation, we generated a highly pigmented melanoma cell line (MNT-1) deficient in the NPC1 protein. The NPC1-KO MNT-1 cells were generated using the CRISPR/Cas9-mediated gene targeting system and underwent single clone selection and immunoblotting analysis. We selected four out of the 30 clones tested that lacked NPC1 expression for further analysis. In contrast to the WT MNT-1 cells (MNT-WT), the NPC1-KO clones were devoid of the NPC1 protein, as shown by Western blotting analysis (Fig. 1*A*). One of the hallmarks of NPC cellular phenotypes is the increased relative lysosomal volume, due to cholesterol and glycosphingolipid accumulation (18, 19). To evaluate relative acidic compartment volume, we stained the four positive cell clones with LysoTracker green and analyzed them by flow cytometry. In the NPC1-KO cells the lysosomal volume was increased in all four clones at least two-fold relative to MNT-WT cells (Fig. 1*B*). Confocal fluorescence microscopy staining with antibody against lysosome-associated membrane protein (LAMP-2) (Fig. 1*C* and quantification in Fig. 1*D*), further indicates an expanded late endosomal–lysosomal compartment in NPC1-depleted cells. This was supported by the upregulation of LAMP-2 expression assessed by the Western blot analysis (Fig. 1*E*). Moreover, the mature form of cathepsin D determined by Western blotting was also elevated in NPC1-KO cell line consistent with unaltered lysosomal function (Fig. 1*F*).

The lack of NPC1 protein leads to unesterified cholesterol and sphingolipid accumulation within the late endocytic and lysosomal compartment (24, 25). Moreover, other studies demonstrated that the transport of TYR and TYRP-1 to the melanosome was influenced by glycosphingolipid level (26). Therefore, the dysregulation of lipid pathways can impact the pigmentation process (27). For example, glucosylceramidase (GlcCer) plays an essential role in melanosomal protein sorting by modifying the pH of the TGN lumen and thus promoting TYR and TYRP-1 oligomerization (28).

We therefore performed biochemical analysis to quantify the different lipids storage in NPC1 deficient melanoma cells. Cholesterol increase in the NPC1-KO cell line relative to WT control was measured using Amplex Red (Fig. 2*A*). HPLC analysis of 2-AA labeled glycosphingolipids (GSLs)-derived glycans revealed that there was increase in GM2, GM3, GD3, GM1b, GD1b, and GT1b (Fig. 2, *B–E*). Depending on the cell line, different GSLs were found to be accumulating in the endolysosomal pathway and we noticed that, in comparison to human fibroblasts, in melanoma cells there is a greater diversity of GSLs species (29). Despite the imbalance of different lipids in NPC1-KO cell line, GlcCer was present at similar levels in both cell lines (Fig. 2*F*).

The characterization of NPC1-KO *versus* MNT-WT cells confirmed that the newly created melanoma cell line recapitulates the NPC cellular phenotypes in terms of increased lysosomal volume and intracellular lipids accumulation. The generated KO cell line (clone 2) was used in subsequent experiments to investigate the role of NPC1 in the pigmentation process.

The pigmentation process of MNT-1 melanoma cells is impaired in the absence of NPC1

We noticed that in the absence of the NPC1 protein, the pigmentation of the MNT-1 melanoma cell line is impaired (Fig. 3*A*). MNT-WT cells were dark brown, almost black, whereas the color of the NPC1-KO cells was light brown. These findings prompted us to further evaluate the fate of TYR in NPC1-KO cells. Western blot analysis showed significantly lower levels of TYR in the two clones of NPC1-KO cells analyzed than the MNT-WT cells (Fig. 3*B*). Moreover, NPC1 silencing by RNAi in MNT-WT cells recapitulated the observed changes at the protein level, defined by a significantly decreased level of TYR (Fig. 3*C*). By expressing NPC1 in KO cell line, the effect of NPC1 on TYR protein levels was reversed, even though the differences were not statistically significant (Fig. 3*D*). Interestingly, among several melanoma cell lines with different pigmentation status (Fig. S1*A*), NPC1 protein is significantly more abundant in MNT-1 cells, the highly pigmented cells in which TYR is well expressed than the amelanotic cells (A375 and SKMEL28) that lack mature TYR (Fig. S1*B*). This could suggest that in cells producing more pigment there is a more stringent requirement for NPC1 function, although other biomarkers are more relevant

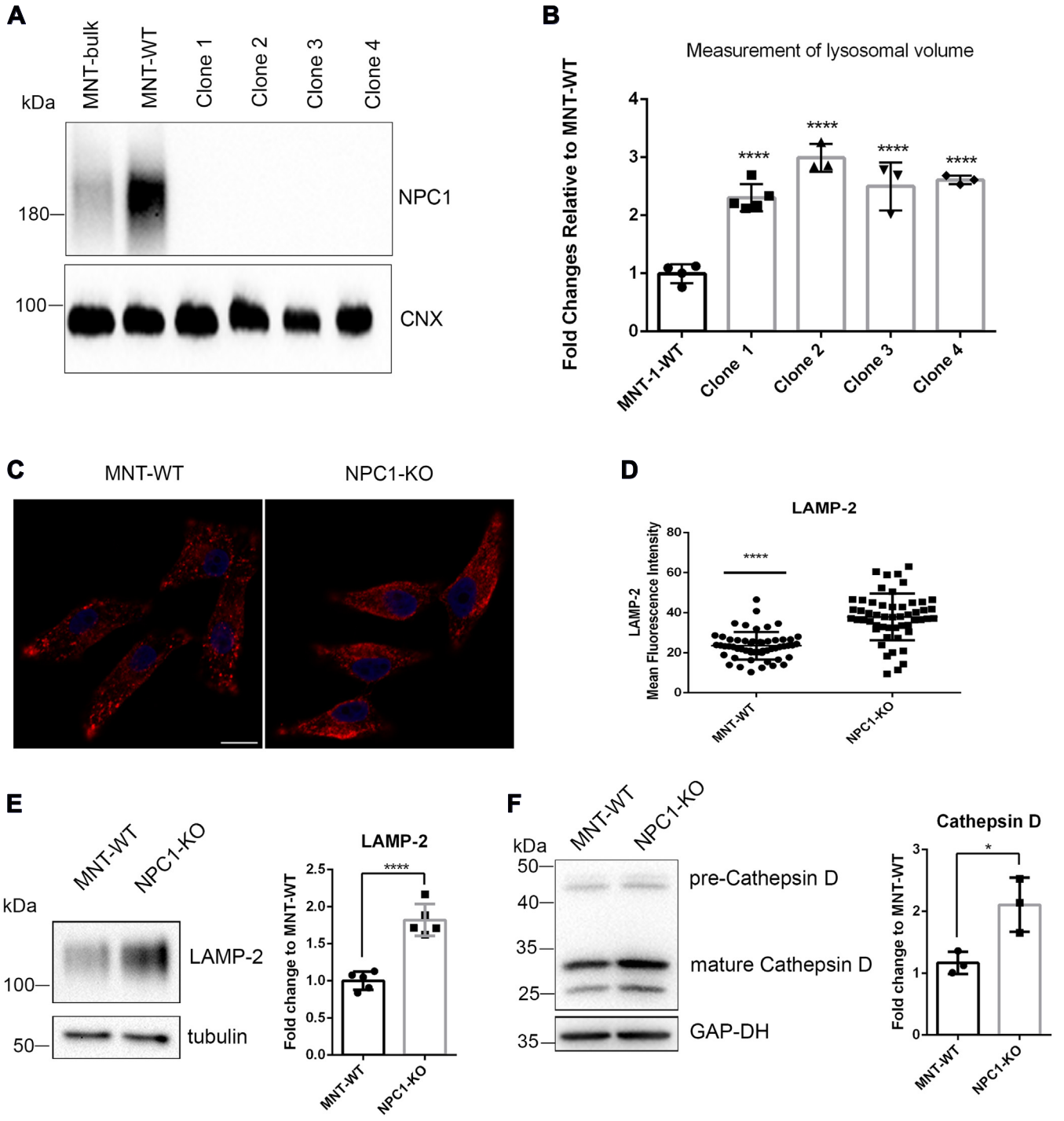

Figure 1. Generation of the NPC1-KO cell line. *A*, immunoblot analysis of NPC1 protein in MNT-WT, MNT-bulk, and NPC1-KO (four clones). Calnexin (CNX) was used as loading control. *B*, relative lysosomal volume of NPC1-KO cells (four clones) to MNT-WT cells measured by LysoTracker staining and FACS analysis. Data analysis was based on mean fluorescence of three independent experiments and represented as mean ± SD (one-way ANOVA analysis; ****$p < 0.0001$). *C*, immunofluorescence staining with anti-LAMP-2; the scale bar represents 10 μm. *D*, graphic representation of mean fluorescence intensity of LAMP-2 immunostaining, n = 52 cells (two-tailed student's *t* test; ****$p < 0.0001$). *E* and *F*, immunoblot analysis and quantification of LAMP-2 (*E*) and cathepsin D (*F*) in MNT-WT *versus* NPC1-KO (clone 2). Band densitometry plot of LAMP-2 (n = 5 biological replicates) and cathepsin D (n = 3 biological replicates) was represented as mean ± SD. Two-tailed Student's *t* test; ****$p < 0.0001$,*$p < 0.05$. FACS, fluorescence-activated cell sorting; LAMP, lysosome-associated membrane protein; NPC1, Niemann–Pick type C1.

for pigmentation, as we recently reported (30). Co-immunoprecipitation studies using the NPC1 antibody revealed a possible direct interaction between TYR and NPC1 (Fig. 3*E*). Next, we have evaluated the activity of TYR in gel and the decreased activity of TYR in the NPC1 deficient cells is seemingly linked to its reduced protein expression level (Fig. 3*F*). To investigate whether there is a downregulation of TYR at transcriptional level, we assessed its gene expression by real time quantitative reverse transcription PCR. The amount of TYR mRNA in NPC1-KO cells was not significantly

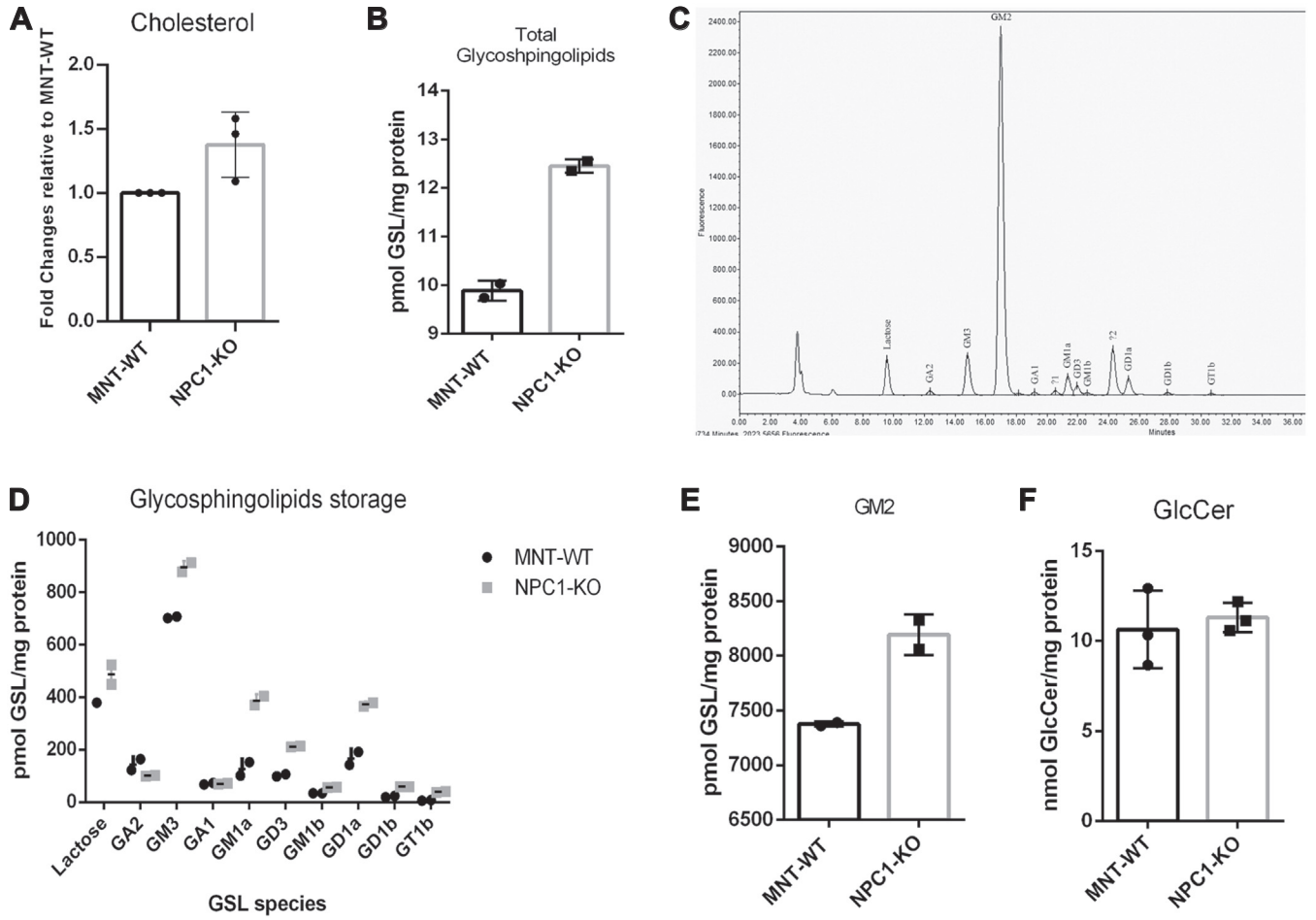

Figure 2. Characterization of the lipid storage phenotypes in the NPC1-KO cell line. *A*, cholesterol measurement by Amplex Red assay, data are presented as the mean ± SD, MNT-WT *versus* NPC1-KO, n = 3 biological replicates. *B*, *D*, and *E*, assay for total GSLs (*B*), for different GSL species (*D*) and for GM2, the main storage species (*E*) by HPLC, n = 2 biological replicates. *C*, representative GSLs trace from MNT-WT cells. *F*, the mean ± SD of GlcCer in MNT-WT and NPC1-KO, n = 3 biological replicates. NPC1, Niemann–Pick type C1; GlcCer, glucosylceramidase; GSL, glycosphingolipid.

changed compared with the one in MNT-WT cells (Fig. 3*G*). In addition, we have probed microphthalmia-associated transcription factor (MITF), the main regulator of the melanogenesis enzymes gene expression (31), which did not show significant alteration in KO cells (Fig. 3*H*). Indeed, MITF levels in the two cell lines were comparable, suggesting that the absence of NPC1 does not induce modifications during transcription of the pigmentation genes. Moreover, due to the cholesterol influence on pigmentation and MITF signaling (32), we tested whether cholesterol depletion would rescue the phenotype in NPC1-KO cell lines. Cells depleted in NPC1 displayed a significantly lower lysosome volume, compatible with the partial rescue of the NPC phenotype upon treatment with 2-hydroxypropyl-β-cyclodextrin, an entrapping cholesterol drug used in NPC treatment (33) (Fig. S2*A*). However, neither the expression of TYR and PMEL17 nor the pigmentation status of these cells were modified (Fig. S2, *B* and *C*). These results suggest that cholesterol is not the primary cause of pigmentation defect in NPC1-KO cells.

Furthermore, Western blot analysis revealed decreased levels of two other melanosomal enzymes involved in melanin biosynthesis, namely TYRP-1 and DCT (Fig. 3, *I* and *J*). In addition to its downregulation, DCT protein exhibited a different glycosylation pattern in NPC1-KO cells, with an increase in the high mannose, immature protein (low molecular band) relative to the fully glycosylated DCT (high molecular weight band). Therefore, in the absence of NPC1, the pigmentation process is reduced, concomitant with a reduction in the expression of TYR that is not modified during transcription or translation, but rather at the posttranslational level.

Proteomic analysis of NPC1-KO cells by nanoLC-tandem mass spectrometry

To gain further insights into the function of the NPC1 protein in melanogenesis, we analyzed the WT and KO cells by mass spectrometry (MS)-based proteomics. We used a method that we described previously (34) in which the cell lysates were separated in a first dimension by SDS-PAGE, the separated bands were digested to peptides and injected into the nanoLC coupled MS. Principal component analysis reveals two main distinct clusters

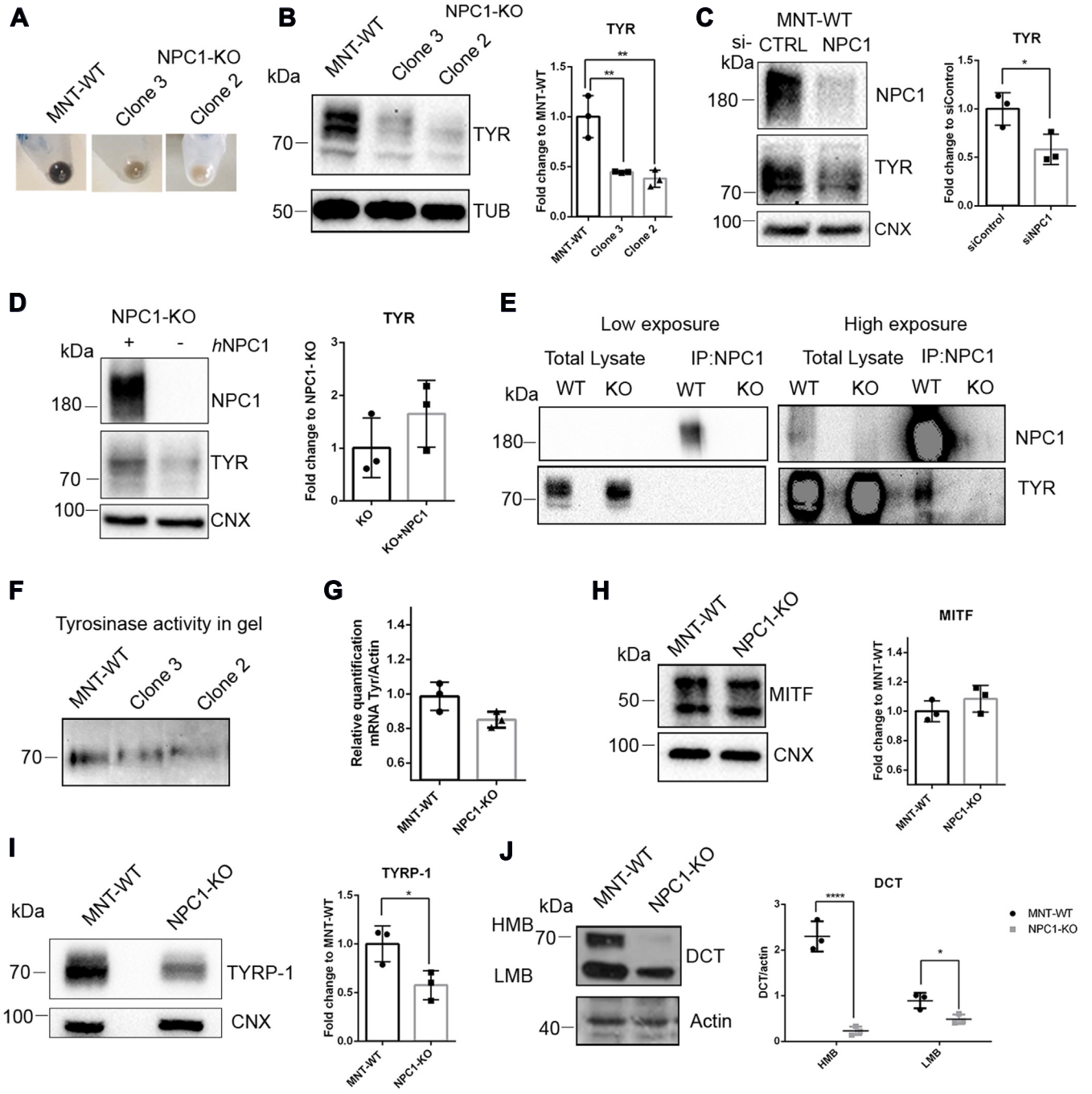

Figure 3. NPC1-KO cells present pigmentation defects. *A*, visual comparison of MNT-WT and NPC1-KO cell pellets. *B*, *C*, and *D*, immunoblot analysis and quantification of TYR in NPC1-KO (clone 3 and 2) *versus* MNT-WT cells (*B*), in MNT-WT cells transfected with siControl (CTRL) or with siNPC1 (*C*) and in NPC1-KO cells transfected with empty vector—pcDNA3.1+ or with *h*NPC1pcDNA3.1+ (*h*NPC1) (*D*). Intensities of TYR protein bands were quantified and represented as mean ± SD (two-tailed Student's *t* test; $^{**}p < 0.01$; $^{*}p < 0.05$, n = 3 biological replicates). *E*, co-immunoprecipitation of NPC1 protein using rabbit anti-NPC1 antibody in MNT-WT and NPC1-KO cell lysates was assessed. The resulted immunocomplexes were eluted with LB, and NPC1 and TYR were visualized by immunoblotting (n = 3 biological replicates). *F*, in-gel analysis of TYR activity. *G*, TYR relative gene expression level determined by semi-quantitative qRT-PCR, n = 3 biological replicates. *H–J*, immunoblot analysis and quantification of MITF (*H*), TYRP-1 (*I*), and DCT (*J*) protein levels normalized to CNX or actin, divided by WT average and represented as mean ± SD, n = 3 biological replicates. CNX, calnexin; DCT, dopachrome-tautomerase; MITF, microphthalmia-associated transcription factor; NPC1, Niemann–Pick type C1; qRT-PCR, real time quantitative reverse transcription PCR; TYR, tyrosinase; TYRP, tyrosinase-related protein.

corresponding to MNT-WT and NPC1-KO cells, respectively, indicating the variation in protein expression between samples (Fig. 4*A*). This proteomic-based approach confirmed the absence of NPC1 protein in the KO cell line and revealed that 57 proteins were significantly modified in NPC1 deficient cells, with 27 proteins upregulated and 30 proteins downregulated (Fig. 4*B* and Table S1). Among the significantly upregulated proteins in the NPC1-KO cell line, we found the lysosomal protein LAMP-2 that was previously reported to be elevated in NPC1 deficient cells (35). We also identified significantly elevated levels of

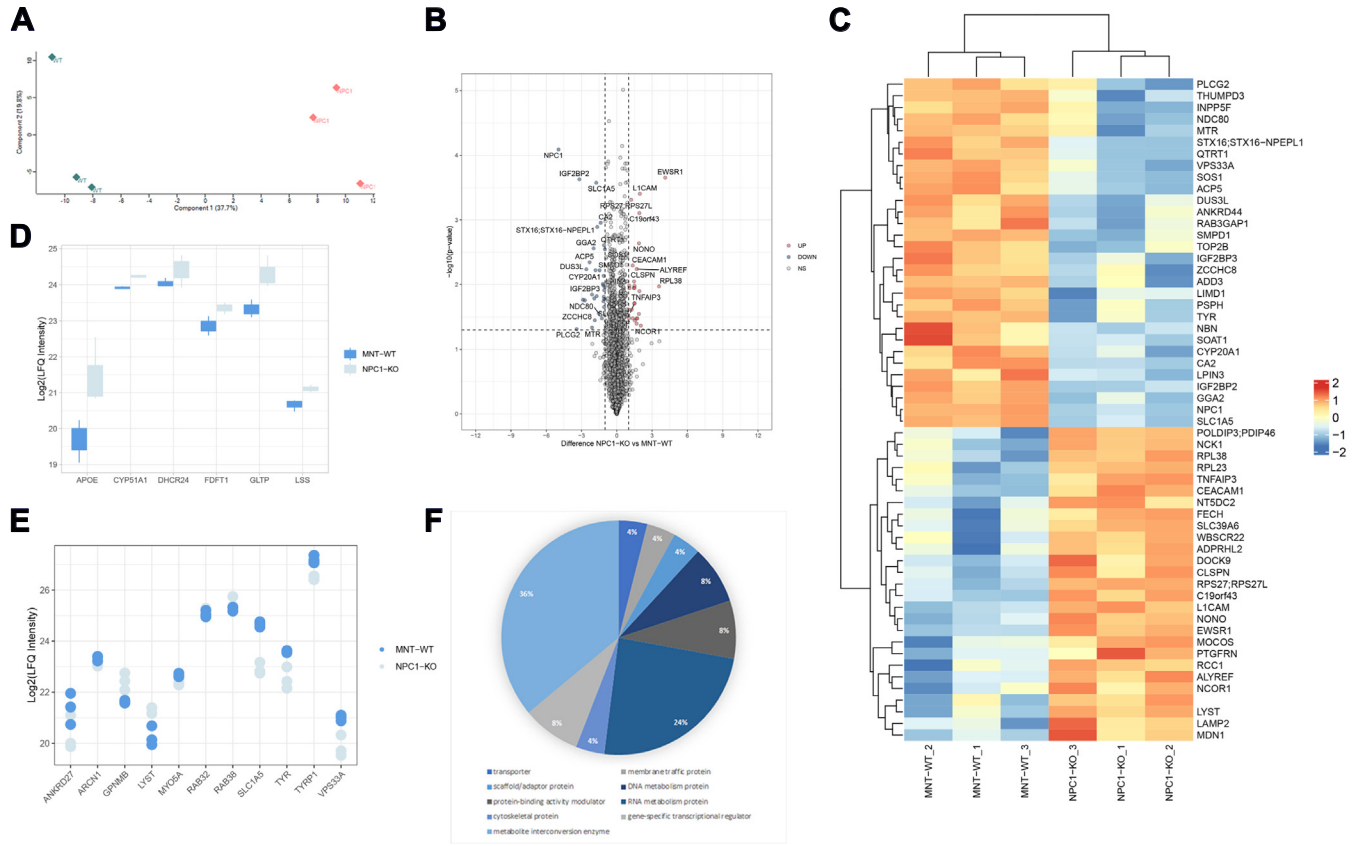

Figure 4. Proteome analysis of MNT-WT *versus* NPC1-KO cells by mass spectrometry. *A*, principal component analysis (PCA) plot showing clustering of replicates according to their characteristics. *B*, volcano plot indicating protein expression differences of MNT-WT *versus* NPC1-KO according to two sample *t* test ($p < 0.05$ and absolute log2FC ≥ 1), n = 3 biological replicates. *C*, heatmap of log2 transformed LFQ intensity values showing the statistically significant upregulated and downregulated proteins in NPC1-KO cell line. *D*, box plot of log2 transformed LFQ intensity values of upregulated proteins involved in lipid metabolism. *E*, pie chart presenting protein classes of significantly downregulated protein in NPC1-KO cell line based on the Panther database. *F*, dot plot of log2 transformed LFQ intensity of selected proteins belonging to melanogenesis pathway. LFQ, label-free quantitation; NPC1, Niemann–Pick type C1.

proteins implicated in macromolecule biosynthetic processes (ESWR1-EWS RNA binding protein 1, NONO-Non-POU domain-containing octamer-binding protein, ALYREF-THO complex subunit 4, NCOR1-nuclear receptor corepressor 1, CLPSN-Claspin, RPL23 60S-ribosomal protein L23, RPL38–60S ribosomal protein L38, RPS27–40S ribosomal protein S27) and in intracellular transport (SLC39A6-zinc transporter ZIP6, LYST-lysosomal-trafficking regulator) (Fig. 4*C*). Additionally, six proteins related to lipid metabolism were increased in the NPC1-KO cell line, among them apolipoprotein E (ApoE) (Fig. 4*D*). Interestingly, ApoE protein is also involved in the melanogenesis process as a regulator of PMEL17 maturation (36). The PANTHER classification system was used to categorize the downregulated proteins related to their protein class and molecular function. We found that 31% of the significantly downregulated proteins belonged to metabolite interconversion enzymes (PSPH-phosphoserine phosphatase, ACP5-tartrate-resistant acid phosphatase type 5, SOAT1-sterol O-acyltransferase 1, CYP20A1, PLCG2-1-phosphatidylinositol 4,5-bisphosphate phosphodiesterase gamma-2, CA2-carbonic anhydrase 2, SMPD1-sphingomyelin phosphodiesterase 1, TYR, INPP5F-inositol polyphosphate-5-phosphatase F) (Fig. 4*E*). Three of them are localized in lysosomes (SMPD1 and ACP5) or early endosomes (INPP5F) and SMPD1 is known also to play a role in lipid metabolism. Moreover, some significantly decreased proteins in NPC1-KO cells are involved in vesicular transport: STX16 (syntaxin 16), VPS33A (vacuolar protein sorting-associated protein 33A) and SLC1A5 (neutral amino acid transporter B (0)). STX16 plays a role in the transport from late endosome to TGN, while VPS33A is involved in the endolysosomal pathway (37, 38). Notably, two of these significantly downregulated proteins, TYR and SLC1A5, localize mainly to melanosomes. Several proteins related to cell pigmentation that may show an impairment of the melanogenesis pathway were plotted in Figure 4*F*.

Taken together these data indicate that in the absence of the NPC1 protein, there were not dramatic differences at the proteome level, although the expression of some proteins was enhanced while some others were reduced. However, validating the initial antibody quantification, there was a significant decrease in the proteins that synthesize melanin (TYR, TYRP-1, and so on), but not in those responsible for melanosomal matrix generation (PMEL17).

TYR processing and degradation is altered in NPC1-KO melanoma cells

The absence of melanin is probably due to the mislocalization or degradation of TYR which catalyzes the

L-tyrosine oxidation to 3,4 dihydroxy-L-phenylalanine (DOPA) and further to Dopachrome, a product able to polymerize and give rise to melanin. Hence, we investigated the maturation process of this glycoprotein, that involves the conversion of its high-mannose N-glycans (endoglycosidase H [Endo H] sensitive) acquired in the ER, into complex N-glycans (Endo H resistant) in medial Golgi. Using Endo H digestion, we found a double band distribution in SDS-PAGE, an Endo H resistant and an Endo H sensitive one (Fig. 5*A*). Complex N-glycans acquired post ER processing were

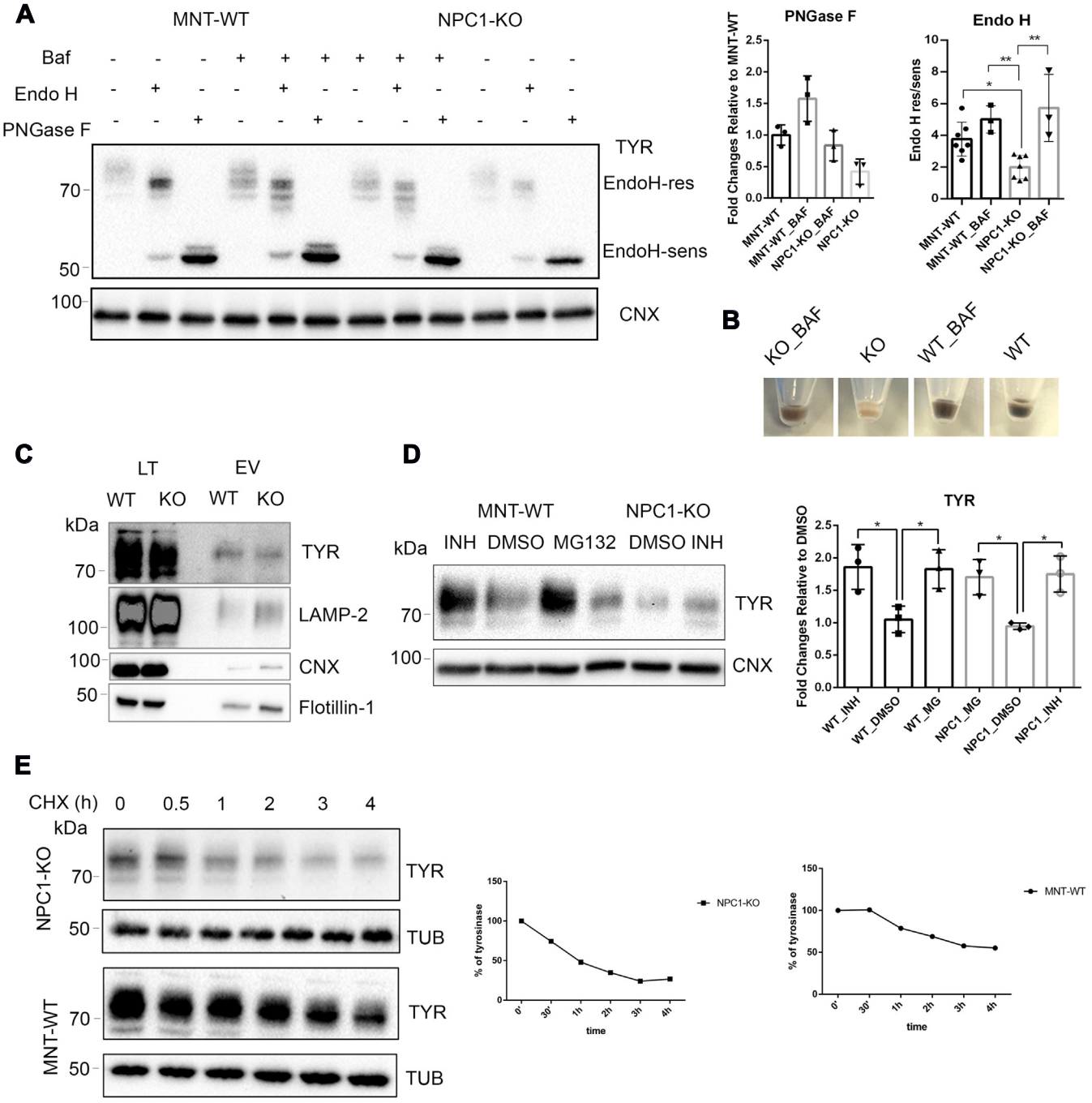

Figure 5. NPC1 impairs TYR processing and degradation. *A*, cells were untreated or treated with bafilomycin A (100 nM, 5 h) and analyzed by Western blotting for TYR N-glycan processing after Endo H and PNGase F glycosidase treatment of cell lysates. Relative expression levels of PNGase F-sensitive TYR and the ratio of Endo H-resistant to Endo H-sensitive TYR were plotted. Quantitative representation as mean ± SD of relative protein expressions and the ratio of Endo H resistant to Endo H sensitive bands (one-way ANOVA analysis; *$p < 0.05$, **$p < 0.01$, n = 3 biological replicates). *B*, visual comparison of cell pellets of MNT-WT and NPC1-KO cells untreated or treated with bafilomycin A1 (100 nM, 5 h). *C*, immunoblot analysis for TYR, LAMP-2, and CNX in cell lysates and in the enrichment of secreted extracellular vesicles from culture supernatant. *D*, effect of MG132 (50 μM, 5 h) or inhibitor mix (INH = 14.5 uM leupeptin and 106 uM pepstatin, 5 h) cell treatment on TYR expression, analyzed by Western blotting and densitometry, represented as fold change relative to cells treated with DMSO. Quantitative representation as mean ± SD of relative protein expression, n = 3 biological replicates (one-way ANOVA analysis; *$p < 0.05$). *E*, CHX treated MNT-WT and NPC1-KO cells analyzed by immunoblotting for TYR normalized to tubulin and graphic representation of TYR degradation rate as a percentage of control (CHX, 0 h) (n = 2 biological replicates). CHX, cycloheximide; CNX, calnexin; DMSO, dimethyl sulfoxide; Endo H, endoglycosidase H; LAMP, lysosome-associated membrane protein; NPC1, Niemann–Pick type C1; PNGase F, peptide-N glycosidase F; TYR, tyrosinase.

removed by digestion with peptide-N glycosidase F (PNGase F), giving rise to a complete deglycosylated protein form (Fig. 5*A*). Treatments were performed on cells treated with 100 nM bafilomycin A1, a macrolide that inhibits endolysosomal acidification, and therefore lysosome-associated degradation (39). The Figure 5, *A* and *B* show that bafilomycin A1 treatment resulted in an increase of TYR expression level and a rescue in pigmentation of NPC1-KO cells. To rule out differences in antibody recognition due to different TYR glycoforms, we measured the level of the deglycosylated polypeptide of TYR obtained after treatment with PNGase F (Fig. 5*A*). TYR appeared to be elevated in the presence of bafilomycin A1 and in the NPC1-KO cells the rescued amount of TYR was higher for both, MNT-WT and NPC1-KO cells. The ratio between Endo H resistant and sensitive fractions was significantly lower in NPC1-KO cells compared with the WT cells, revealing that the immature form of TYR is increased in the absence of NPC1. This might indicate that in NPC1-KO cells there is a defective or delayed posttranslational processing in the Golgi compartment or that mature TYR is more rapidly degraded. After treatment with bafilomycin A1 and digestion with Endo H, TYR presents two more intermediate complex glycosylated forms. In contrast to the Endo H-sensitive band that corresponds to the molecular species in which all 6 N-glycans were high mannose, the Endo H-resistant bands reveal a ladder of Golgi species with less high mannose immature N-glycans. This may suggest that in the presence of bafilomycin A1, TYR transit through the Golgi is faster and some N-glycans remain unprocessed to complex structures. Moreover, bafilomycin A1 reduces the TYR degradation process in both cell lines. The ratio between the all Endo H-resistant *versus* sensitive forms of TYR was similar in NPC1-KO and MNT-WT cell lines. However, the mature TYR is less degraded in the presence of bafilomycin A1 in WT than in the KO cells, indicating that there are post Golgi events affecting TYR degradation in the NPC1 defective cells (Fig. 1*A*). Thus, preventing acidification along secretory/endolysosomal compartment by bafilomycin partially restored TYR maturation and stability in NPC1-KO melanoma cells. TYR seems to be able to reach post Golgi membrane compartments where it can initiate some melanin biosynthesis and pigmentation in the NPC1-KO cells.

To gain insight into the TYR fate in the two cell lines, we further evaluated the TYR pool secreted by melanoma cells. The culture media were collected after 72 h and the extracellular vesicles were analyzed by Western blotting. As shown in Figure 5*C*, although LAMP-2 is more secreted in NPC1-KO cells, TYR levels are lower in the secreted extracellular vesicles. This indicates that the low expression level of TYR is not due to a higher pool in the extracellular medium, but to an intracellular sequestration and degradation process. Flotillin-1, which is an exosome component (40), was present in exosomes isolated from both melanoma cells (Fig. 5*C*), suggesting that the secretion process is not impaired in the absence of NPC1.

To further understand the TYR degradation process, we studied the response of TYR expression levels to proteasome and lysosome inhibitors in NPC1-KO and MNT-WT cells. Cells were incubated for 5 h with either MG132, a proteasomal inhibitor, or with a mix of pepstatin A and leupeptin, to inhibit lysosomal enzymes (41). In both treatment conditions, elevated levels of TYR were detected by Western blot, suggesting a proteasomal but also a lysosomal degradation pathway of TYR in the two melanoma cell lines (Fig. 5*D*). Furthermore, the kinetics of TYR degradation in the two cell lines was assessed by treatment with cycloheximide, a protein biosynthesis inhibitor that prevents translational elongation (42). MNT-WT and NPC1-KO cells were harvested at different time points (0, 0.5, 1, 2, 3, and 4 h) after incubation with cycloheximide and the expression of TYR was examined by quantitative Western blot analysis. As shown in Figure 5*E*, the immunoblot and the quantification revealed a decreased half-life of TYR in the NPC1-KO cells (1 h) compared to MNT-WT (4 h). We therefore assume that reduced levels of TYR are processed to mature protein revealing poor quality control in the secretory pathway of the NPC1-KO cells resulting in an accelerated degradation of TYR. The altered N-glycosylation occurring at the Golgi compartment together with the maturation process rescuing during acidification, would indicate a late endosomes-TGN impaired traffic in the absence of NPC1 leading to a misrouting of TYR toward degradation.

TYR and PMEL17 fibrils are redistributed in immature melanosomes in NPC1-KO cells

To further investigate the putative alterations in melanosome biogenesis in NPC1 deficient cells, we have studied the subcellular localization of several proteins associated with endolysosomes and melanosomes. We analyzed the distribution of TYR by confocal immunofluorescence microscopy in the two cell lines. In MNT-WT cells, TYR immunostaining appeared as punctuate structures scattered throughout the cytoplasm, a significant pool being concentrated in the perinuclear region (Figs. 6 and S3). Bright field images showed TYR labeling coinciding with the pigment granules accumulated in the juxtanuclear region, but also with those distributed at the cell periphery and cell tips, thus confirming the steady state localization of TYR to pigmented, mature melanosomes (Fig. S3). In contrast, in NPC1-KO cells, not only was the intensity of the TYR staining lower, but also its intracellular distribution was strikingly different. The juxtanuclear TYR signal was significantly depleted, whereas its localization was concentrated along extended regions at the cell periphery, close to the plasma membrane. At the same time, these cells lacked mature, highly pigmented melanosomes.

Most TYR detected in MNT-WT cells co-localized extensively with RAB38 (high Manders' coefficient (43)), a Rab GTPase involved in the regulation of membrane transport to and from mature melanosomes (44) (Fig. 6). By contrast, in NPC1-KO cells, their co-localization appeared to be restricted to the peripheral compartments. A similar effect on the intracellular distribution was observed for TYRP-1, another protein involved in melanogenesis. Moreover, there was a reduction in the fluorescence intensity for TYR and TYRP-1

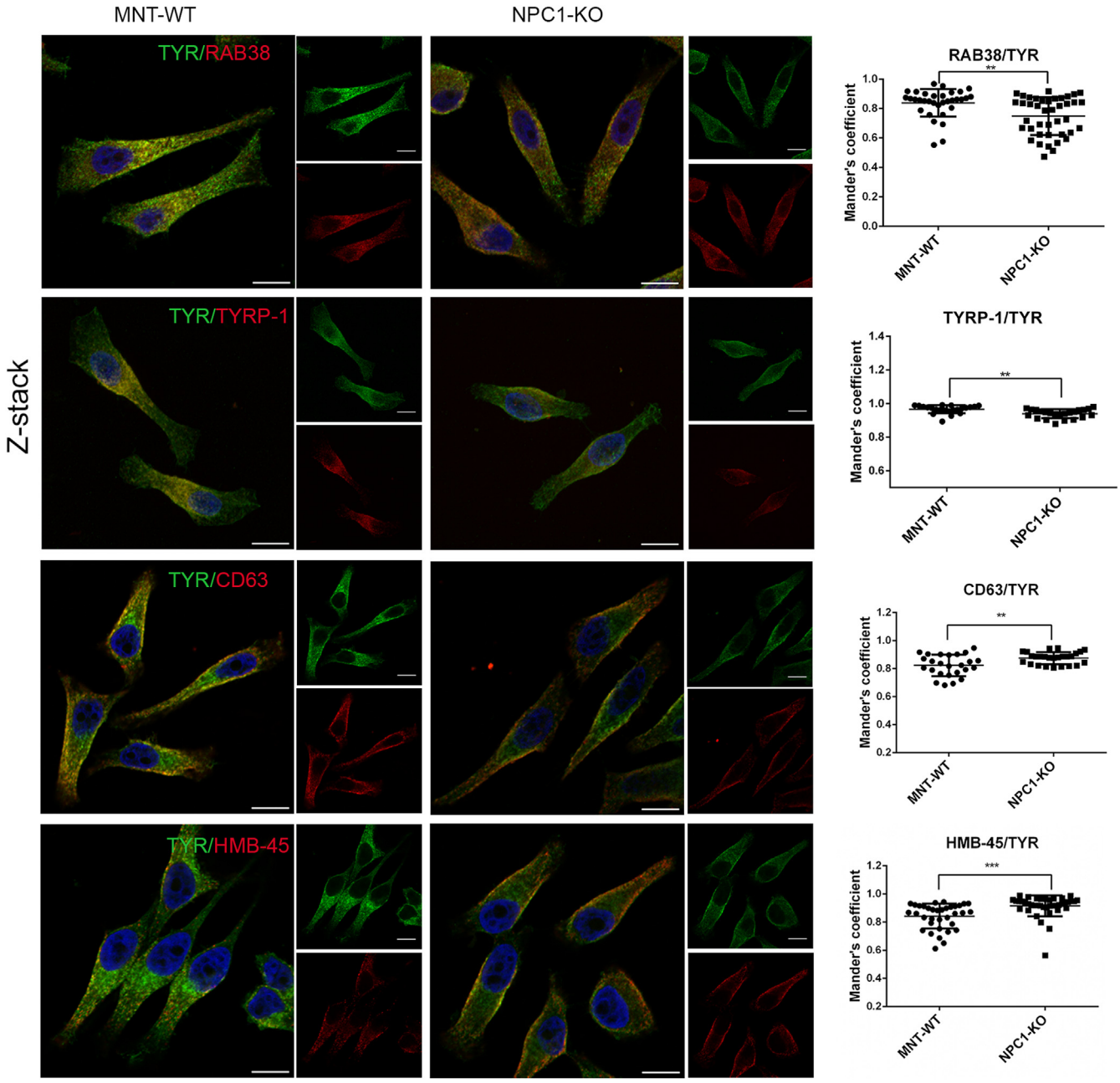

Figure 6. Altered distribution of proteins involved in melanogenesis. Co-localization of TYR with RAB38, TYRP-1, CD63, and PMEL17 (HMB-45) by confocal immunofluorescence microscopy (the scale bar represents 10 μm). The Manders' correlation coefficient was plotted for the measurement of the co-localization of TYR with RAB38 (n = 33), TYRP-1 (n = 22), CD63 (n = 25) and HMB-45 (n = 35). Two-tailed Student's *t* test was applied for statistical analysis (**$p < 0.01$, ***$p < 0.001$). HMB, human melanoma black; TYR, tyrosinase.

detected proteins (Fig. 6). The decrease in pigmentation and the alterations in the expression and subcellular localization of proteins normally associated with mature melanosomes suggest that NPC1 deficiency causes defects in melanosome biogenesis and/or maturation. Since sorting of the melanogenic enzymes to the maturing melanosomes originates from specific endosomal subcompartments, we investigated the morphology of the different organelles in the endocytic pathway using specific markers. The staining for EEA1, a protein associated with early endosomal membrane domains, was not substantially modified in NPC1-KO cells compared with WT MNT-1 cells (Fig. S3). On the other hand, TYR and EEA1 displayed a mutually exclusive localization in both cell lines, with a low Manders' coefficient. In contrast, there was a partial, but evident co-localization of TYR with CD63 (high Manders' coefficient), a tetraspanin present in endolysosomes, as well as in maturing melanosomes, in MNT-WT cells, CD63 being located more peripherally than TYR. In NPC1-KO cells, CD63 staining appeared enriched at extended sites in the cell periphery where TYR was also present (Figs. 6 and S3).

In addition, to further identify early stages in melanogenesis, we assessed the localization of PMEL17, a structural protein

that undergoes sequential proteolytic steps in the Golgi and in an endosomal/premelanosomal compartment, to ultimately generate the fragments that form the fibrillar amyloid matrix of melanosomes (13). We used a pair of antibodies, namely human melanoma black (HMB)-45 and PEP-13, to distinguish between the different PMEL17 processed forms. HMB-45 antibody recognizes the processed Golgi and post-Golgi forms, and the mature fibrillar PMEL17, while PEP-13 identifies the full-length forms of PMEL17 (P1/P2) and the M-beta peptide, generated in the first steps of PMEL17 processing. The immunofluorescence labeling shows that in both cell lines PEP-13 reactive PMEL17 was not co-localized with the mature, HMB-45 reactive PMEL17. While we did not detect a significant difference in PEP-13 staining, the HMB-45 reactive PMEL17 appeared redistributed to the cell periphery in NPC1-KO cells (Fig. S3). In MNT-WT cells, HMB-45 exhibited partially co-localization with TYR on discrete punctate structures, mainly located in the cell periphery, but also intracellularly, however in NPC1-KO cells, both proteins were shifted peripherally where they partially co-localized. There is an increase in the co-localization of TYR with HMB-45 in NPC1-KO cells (high Manders' coefficient) as shown in Figure 6.

The abnormal localization of PMEL17, prompted to us to investigate whether there are differences in its maturation process and fibril formation. We found that the expression of the immature (P1/P2) and M-beta forms of PMEL17, recognized by PEP-13 antibody were not modified in the absence of NPC1 protein (Fig. 7*A*). However, a ladder of fibril-associated fragments containing the repeat domain (RPT)appeared highly expressed in the absence of NPC1 suggesting cellular alterations in these cells that favor the aberrant production of the mature PMEL17 (Fig. 7*A*). The residual insoluble PMEL17 aggregates, extracted in more stringent detergent conditions, run with similar fibril patterns in gel. The immunoblot analysis showed that there was a statistically significant increase in both soluble and insoluble PMEL17 forms in NPC1-KO compared with MNT1-WT cells. The accelerated fibril formation could occur at the plasma membrane or in the endosome/multivesicular bodies during PMEL17 maturation process requiring a transient traffic to the plasma membrane before the transfer

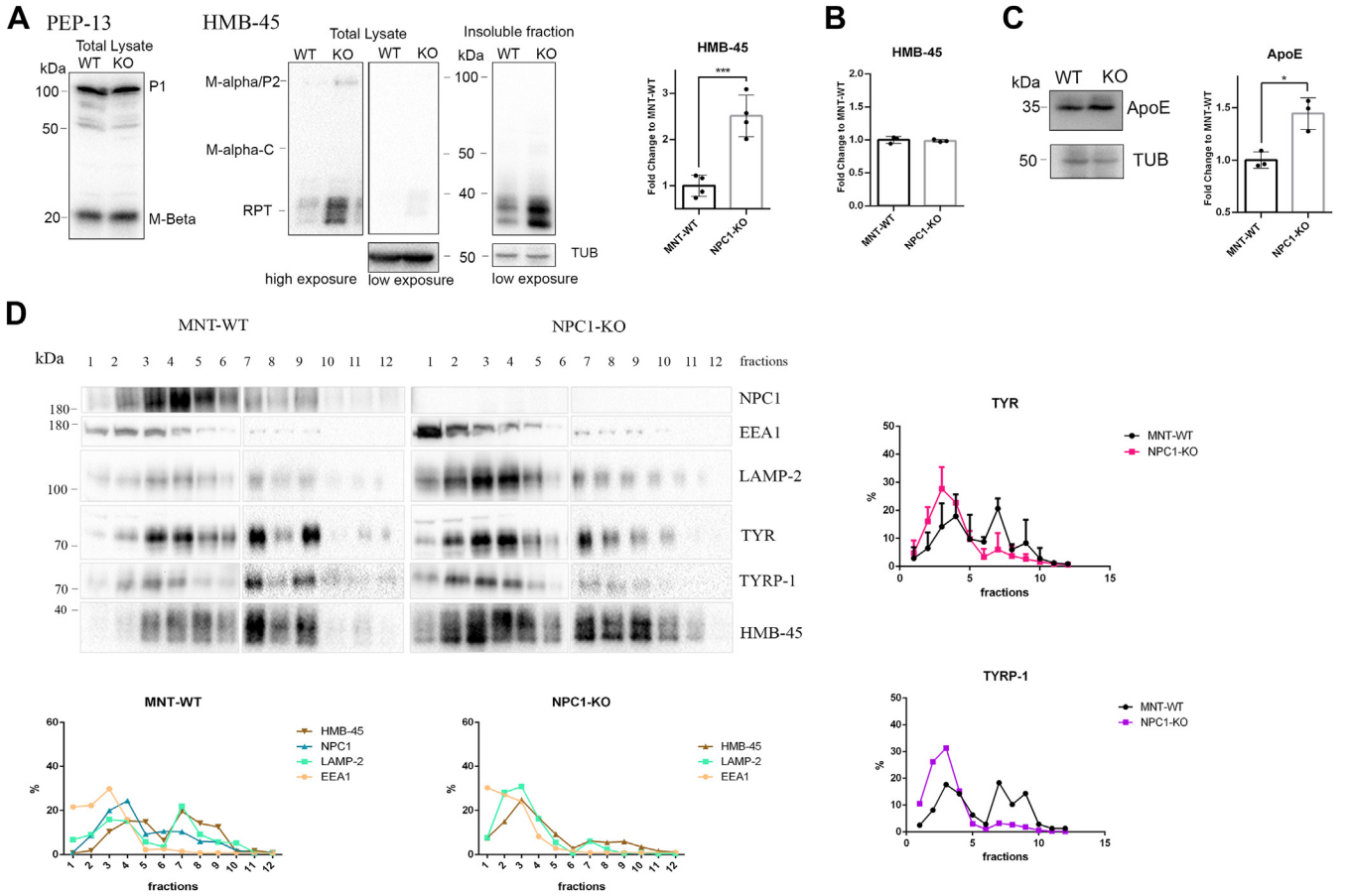

Figure 7. Investigation of the PMEL17 pathway in the absence of NPC1. *A*, immunoblot analysis of PMEL17 protein recognized by PEP-13 (immature PMEL17-P1 and M-beta) and HMB-45 (M-alpha/P2, M-alpha-C and RPT) antibodies. The insoluble fraction was extracted with 1% SDS and 50 mM DTT and boiled at 95 °C. The KO HMB-45 positive fraction was normalized to loading control, and divided by WT average and the relative fold change was represented as mean ± SD (Two-tailed Student's *t* test; ***$p < 0.001$, n = 3 biological replicates). *B*, the surface expression of PMEL17 analyzed by flow cytometry represented in a bar plot as the median of fluorescence related to MNT-WT. *C*, immunoblot analysis of ApoE protein and graphical representation as mean ± SD of relative protein expressions(Two-tailed Student's *t* test; *$p < 0.05$, n = 3 biological replicates). *D*, subcellular fractionation of MNT-WT and NPC1-KO cell homogenates on a sucrose gradient. Twelve fractions were collected and analyzed by immunoblotting with antibodies directed against NPC1, EEA1, LAMP-2, TYR, TYRP-1, and HMB-45. Graphic representation of quantified proteins expression level as mean of two independent experiments. For TYR, three independent replicates were quantified and plotted as mean ± SD. ApoE, apolipoprotein E; HMB, human melanoma black; LAMP, lysosome-associated membrane protein; NPC1, Niemann–Pick type C1; TYR, tyrosinase; TYRP, tyrosinase-related protein.

to early endosome/premelanosomes (45). The possible enrichment of mature PMEL17 at the cell membrane was measured by flow cytometry. As shown in Figure 7*B*, the surface expression of PMEL17 protein was similar in both cell lines. Therefore, NPC1-KO cells display a raise in the mature PMEL17 protein, which is accumulated in premelanosomes/immature melanosomes. Of interest, ApoE, a regulator of amyloid fibril generation (36) had increased expression in NPC1-KO cells in Western blot analysis consistent with the proteomics data (Fig. 7*C*).

In an attempt to characterize the localization of the most prominent pigmentation factors, melanin synthesizing TYR and the PMEL17 fibrils forming the matrix for melanin deposition, we performed cell fractionation and ultracentrifugation experiments. We used a sucrose-density gradient to separate the high-dense melanosomes from the low-density immature melanosomes and other cellular compartments (46). The data presented in Figure 7*D* shows TYR in MNT-WT distributed in low- and high-density fractions over the gradient. One peak corresponds to fractions enriched in proteins from late endosomal/lysosomal and related organelles, namely LAMP-2 and NPC1 (fractions 3 and 4). The later peaks of TYR likely derived from stage III and IV melanosomes were in the denser fractions of the gradient. A minor pool of TYR was also detected in the first fractions abundant in the early endosomal marker EEA1 and could account for the population of TYR en route to melanosomes (Fig. 7*D*, fractions 1 and 2). In NPC1-KO cells the pool of TYR from the denser fractions were significantly depleted. On the other hand, TYR peak associated with the low-density fractions enriched in premelanosomes/immature melanosomes was consolidated, in parallel with an increase in LAMP-2 content in these fractions. A similar profile was found for TYRP-1, another melanosomal protein. The mature form of PMEL17, recognized by HMB-45 antibody displayed an increased level but also an altered distribution in NPC1-KO cells (Fig. 7*D*). Thus, while in WT cells it was enriched in dense fractions, presumably containing mature melanosomes, in NPC1-KO cells, there was a high abundance in the light fractions with equal distribution in the denser fractions as well. These results suggest that in NPC1 deficient cells TYR and PMEL17 fibrils are found in early stages (I–II) melanosomes and in other low-density compartments and that the normal maturation of melanosomes is compromised.

Discussions

Here, we show that NPC1 has a novel function in regulating cargo traffic toward LROs and in melanosome biogenesis. In melanoma cells lacking the NPC1 protein, the traffic of TYR and TYRPs is diverted from melanosomes toward lysosomes and the cargo is degraded. As a consequence, melanin biosynthesis is reduced followed by the reduced formation of the PMEL17-melanin matrix in early melanosomes, these organelles remain immature affecting dramatically the cells pigmentation process. Interestingly, there are no reported cases of NPC patients with vitiligo or other pigmentation defects; however, it has been reported that NPC1-deficient mice show severe retinal degeneration accompanied by alterations in the retinal pigment epithelium layer (47). In these types of pigment cells that are different from eye melanocytes, melanosomes trafficking is altered with melanosomes being diverted to regions that accumulate lipofuscin causing visual problems. We speculate that the trafficking defects described in this study using highly pigmented cells may either remain undetected in NPC1 patients that retain some residual NPC1 function, or could be aggravated in specific melanocytes in severe cases.

In addition to the cargo traffic diversion, the NPC1-KO cells display the accumulation of lipids, that is, cholesterol and GSLs characteristic of NPC cells. While this may also have contributed to impaired melanosome biogenesis, it is important to note that cholesterol has been reported to affect pigmentation by activating MITF signaling (48), which does not occur in the NPC1-KO cells as found by our Western blot antibodies experiments. Furthermore, the cyclodextrin depletion of cholesterol, while resulting in a reduction in the lysosomal volume of the NPC1 depleted cells, had minor effects on TYR expression and cells pigmentation. As far as GSLss are concerned, only GlcCer was found to alter TYR traffic in melanocytes (26), and although glycosphingolipids, GM2, GM3, Gb4, GM1a, GD3, GM1b, GD1a, GD1b, and GT1b, increase significantly in NPC1 null cells, GlcCer did not accumulate in the absence of NPC1 in these melanoma cells. Hence, the lipid accumulation may not be a direct cause of the pigmentation reduction in the absence of NPC1 but reflect changes in the expression of genes involved in melanin biosynthesis. Besides exosomes secretion, another process involving LRO traffic that involves a multivesicular bodies step before cargo secretion in the extracellular space is not altered by the specific lipid partition in NPC1-KO cells (Fig. 8).

The LC-MS/MS analysis of the proteome of NPC1-KO cells revealed modest alterations in comparison with WT MNT-1 cells, but identified a significant decrease in TYR and TYRP-1. TYR, which is under the transcriptional control of MITF (49–51) is not altered during transcription or translation as shown by the real time quantitative reverse transcription PCR experiments. However, TYR turnover was three times faster, explaining the diminished expression level at steady state and the drastic reduction in melanin synthesis in the KO cells. The investigation of the N-glycosylation process revealed that the ratio of immature *versus* mature TYR is higher in the absence of NPC1, indicating that NPC1 that co-immunoprecipitates with TYR also is involved in its maturation. Given that both TYR and NPC1 are membrane glycoproteins carrying a cytosolic dileucine signal motif, it is likely that they are both sorted from the TGN to a common endocytic compartment, which can further mature into late endosomes or melanosomes (52, 53). Furthermore, TYR maturation requires a number of steps including the passing of ER quality control, for export to the Golgi, the TGN extraction toward the LRO evolving in melanosomes, and a possible retrograde transport step from the first LRO back to TGN for final quality control. This may explain the recovery of TYR expression and melanin synthesis together with abundant

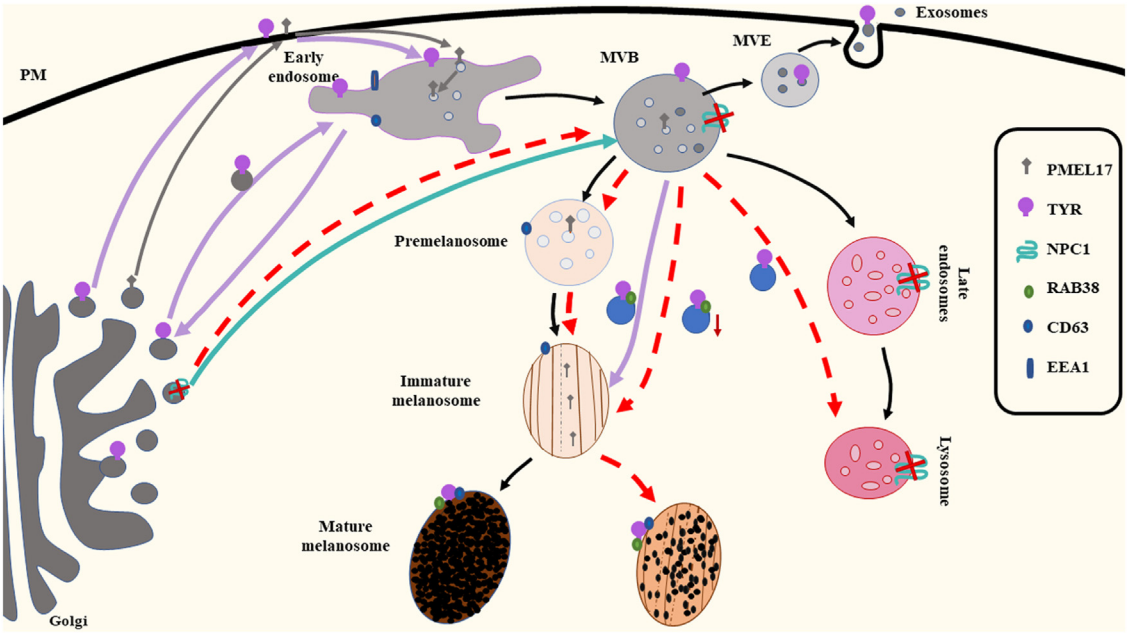

Figure 8. Schematic representation of intracellular TYR trafficking during melanosome maturation. In this model, we propose a model of the mechanism of melanosome biogenesis by highlighting PMEL17 and the TYR pathways in NPC1-KO cells compared to MNT-WT cells. In MNT-WT, as in NPC1-KO cells the PMEL17 protein is trafficked from the TGN to the plasma membrane (PM) and is then endocytosed, while TYR is targeted to early endosomes directly or *via* PM. The early endosomes progressively mature into MVB, from which late endosomes, premelanosome or multiple vesicle exosomes (MVE) are developed. As illustrated, exosome secretion is not affected in NPC1 deficient cells mutant cells, while the pathways which lead to melanosome maturation are impaired in NPC1 KO cells. PMEL17 is sorted to intraluminal vesicles in premelanosome and forms a sheet-like matrix of amyloid fibrils, where melanin can be deposited. In the absence of the NPC1 protein, PMEL17 fibrils accumulates and the maturation of the immature melanosomes is perturbed (*dashed arrows*). In MNT-WT cells, TYR is sorted from the MVB to immature melanosomes, where it initiates the melanin biosynthesis process. In contrast, in NPC1-deficient cells, TYR delivery to immature melanosomes is reduced, due to its target misrouting for lysosomal degradation. The key to the proteins indicated in the figure are presented in the *right hand panel*. The modified pathways in NPC1-deficient cells are indicated by *dashed red arrows*. MVB, multivesicular bodies; NPC1, Niemann–Pick type C1; TGN, *trans*-Golgi network; TYR, tyrosinase.

melanosomes biogenesis in the presence of bafilomycin A1. Further to the inhibition of lysosomal degradation, bafilomycin also inhibits some retrograde traffic pathways between the Golgi and ER and possibly between the LRO and TGN. This could explain the alteration of the N-glycosylation of TYR, that in the presence of bafilomycin A1 displays a new Endo H resistant glycoform that indicates that at least one out of the seven N-glycans is not processed within the medial and *trans* Golgi toward complex N-glycans. This is a glycoform that possibly has been returned from the LRO to the Golgi and rapidly redirected from the TGN toward the precursor LRO for melanosomes, instead of being targeted to lysosomes for degradation (Fig. 8). Besides bafilomycin A1, TYR degradation was rescued by the overexpression of NPC1 in KO cells, thus validating the role of NPC1 in facilitating TYR targeting toward melanosomes in the detriment of lysosome targeting. NPC1 could chaperone TYR and position it in a complex with transporters such as adaptor protein complex-3 and biogenesis of lysosome-related organelles complex 1 (7) required for targeting the melanosomes.

About 60% of TYR was misrouted to lysosomes and degraded (Fig. 5*A*), but the remaining TYR was also mislocalised in the absence of NPC1. The confocal microscopy analysis revealed that while in MNT-WT cells TYR was identified mainly in melanosomes localized in the perinuclear area and dendrite tips, in the NPC1-KO cells, we found nondegraded TYR in rare distal vesicles co-localizing with Rab38, PMEL17, and TYRP-1 but also with CD63. Considering the above markers, it appears that these peripheral organelles are early LRO, such as multivesicular bodies/premelanosomes containing striated fibrils unable to mature further to final melanosomes stage. Since melanin synthesis was not completely abolished, we assume that alternatives routes are available, such as the targeting of TYR to melanosomes *via* the adaptor protein complex-3 transporter (7, 54).

Unlike TYR, PMEL17 is not diverted toward lysosomes, but rather continues to be trafficked toward the LRO from TGN. Interestingly, we found that even if the expression of the full-length polypeptide was similar in both lines according to the PMEL17 antibody recognition, there was a more intense staining with the antibodies recognizing the repeated region RPT specific for fibrils in the absence of NPC1. This may be due to a more efficient process of generation of fibrils or simply to the fact that NPC1-KO cells contain little melanin and the HMB-45 recognition is enhanced in these conditions as previously reported (45). In any case, these data show that PMEL17 amyloid fibrils generation is not impaired by NPC1 deficiency and the maturation of melanosomes is stopped mainly by TYR misrouting. Indeed, the HMB-45 positive organelles were distributed in lower density fractions upon sedimentation ultracentrifugation in KO cells as compared to WT, together with TYR. In WT cells, denser organelles, probably melanosomes were identified as positive for both TYR and PMEL17, validating the conclusion that melanosomes maturation does not occur in these cells. Consistent with this hypothesis is the fact that PMEL17 trafficking toward the plasma membrane,

which occurs before its multivesicular bodies transport (45) was not modified in KO cells, thus validating the nonaltered traffic of PMEL17 (Fig. 8).

In summary, we describe a pigmented cell, MNT-1 NPC1-KO, that despite normal Rab38 function has an altered trafficking of TYR to melanosomes and despite PMEL17 generating the melanosome matrix, melanosome biogenesis is disturbed at an early stage. The pigmentation process is not completely abolished, possibly due to the existence of alternative endocytic routes. In addition to its important role in cholesterol and sphingolipid transport, another function of NPC1 is enabling specific membrane cargo trafficking, such as TYR to facilitate its transport toward a specific LRO lineage distinct from the lysosome. It is thus conceivable that NPC1, itself a multipass transmembrane protein, could associate with different membrane proteins within the TGN and facilitate their traffic to specialized endolysosomal organelles such as TYR to melanocytes.

Experimental procedures

Cell culture

Human MNT-1, A375, SKMEL23, and SKMEL28 cell lines were from the European Collection of Animal Cell Cultures. LAU-ME290 (Me290) is a gift from Professor Romero from the Ludwig Institute of Cancer Research, Lausanne Branch, Switzerland (55). Human MNT-1 cells and A375 cells were cultivated in Dulbecco's modified Eagle's medium (cat: 10566-032) medium supplemented with 10% heat-inactivated (56 °C, 30 min) fetal bovine serum (FBS) (cat: 10270-098) from Gibco (LifeTechnologies), in a humidified atmosphere containing 5% CO2. SKMEL28, SKMEL23, and Me290 cell lines were cultivated in RPMI 1640 medium (cat: 61870-10, Gibco) supplemented with 10% heat-inactivated FBS.

Generation of NPC1 KO cell line using CRISPR/Cas9 system

MNT-1 cells were co-transfected with CRISPR/Cas9 KO-specific plasmids from Santa Cruz Biotechnology (NPC1 CRISPR/Cas9 KO Plasmid (h) (sc-403252) and NPC1 HDR Plasmid (h) (sc-403252-HDR), according to manufacturer's instruction. At 48 h post transfection, the media was changed with fresh Dulbecco's modified Eagle's medium supplemented with 0.5 μg/ml puromycin, a selection antibiotic. Selection efficiency was verified by microscopy of fluorescence. Further, for single-cell cloning, the red fluorescent cells were sorted by flow cytometry and were plated in a 96-well plate. The single cells colonies were transferred onto a 24-well plate and NPC1 expression was verified by immunoblotting.

NPC1 RNAi silencing and NPC1 transfection

2×10^6 MNT-1 cells were seeded in 6-well plate and were transfected with 50 nM NPC1 siRNA or control siRNA-A (sc-37007, Santa Cruz Biotechnology) using lipofectamine 2000. Cells were harvested after 96 h and protein expression was analyzed by Western blot. For rescue experiments 2×10^6 NPC1-KO cells were seeded in 6-well plate and were transfected with further plasmids: pcDNA3.1+ (for control cells) and *h*NPC1pcDNA3.1+ using lipofectamine. Seventy-two hours post transfection cells were harvested and the protein expression was analyzed by Western blot.

Antibodies and reagents

Mouse Anti-TYR (T311, sc-20035, Santa Cruz Biotechnology) antibody was used for Western blot and rabbit anti-TYR antiserum (PEP7, a gift from Dr V. J. Hearing, NCI, National Institute of Health) antibody was used for IF. Rabbit anti-PMEL17 (PEP13) antibody was a gift from Dr V. J. Hearing (NCI, National Institute of Health). Mouse anti-cathepsin D (sc-377299), mouse anti-TYRP-1 (sc166857), goat anti-TRP2/DCT (sc-74439), mouse GAP-DH (sc-81545), mouse anti-Rab38 (sc-390176), rabbit anti-flotillin-1 (sc-25506) and mouse anti-LAMP-2 (sc-18822) antibodies were from Santa Cruz Biotechnology. Rabbit anti-NPC1 (ab108921), mouse anti-MITF (ab80651), rabbit anti-Calnexin (ab22595) and rabbit anti-tubulin (ab18251) antibodies were purchased from Abcam. Mouse anti-HMB-45 (M06340-1) antibody was from Agilent. LysoTracker Green (DND-26 #8783) was from Cell Signaling Technology. Propidium iodide, cycloheximide and 3,4 dihydroxy-L-phenylalanine (L-DOPA, D9628), 2-hydroxypropyl-β-cyclodextrin (H107) were from Sigma-Aldrich. MG132 (sc-201260), leupeptin hemisulfate (sc-295358) and pepstatin A (sc-45036) were from Santa Cruz Biotechnology.

Flow cytometry

Relative lysosomal volumes were measured in MNT-WT *versus* NPC1-KO cells by flow cytometry. Cells were washed twice with PBS and stained with LysoTracker green (200 nM in PBS) for 10 min at 20 °C. The samples were washed with PBS, moved into fluorescence-activated cell sorting (FACS) buffer (10% FBS in PBS) and stained with propidium iodide (1 μg/ml) immediately before FACS analysis. The analysis was performed on a BD FACSVerse Flow Cytometer (BD Biosciences), 10,000 cell events were recorded, and the lysosomal staining was detected on FITC channel. Gating and analysis were performed using Cytobank and the mean fluorescence was plotted using GraphPad.

To measure the surface expression of PMEL17 protein the cells were detached with accutase and were incubated with HMB-45 antibody (1:50) for 30 min. After washing the cells, they were incubated with secondary antibody labeled with AlexaFluor488 and were analyzed on the BD FACSVerse Flow Cytometer (BD Biosciences) with detection on the FITC channel. The data were analyzed using Cytobank (https://community.cytobank.org/cytobank/login) and GraphPad (https://www.graphpad.com/ (Prism6)).

Western blot

To quantify the expression of proteins of interest, Western blotting was performed. Cells were plated prior to the experiment, after 2 days they were harvested and lysed in 1% NP40 buffer containing protease inhibitors (Protease Inhibitor Cocktail) for 30 min on ice and then centrifuged at 14,000 rpm

for 20 min. Total protein from each sample was determined by bicinchoninic acid method. Equal amounts of protein were separated by SDS-PAGE, transferred onto nitrocellulose or polyvinylidene fluoride or polyvinylidene difluoride membranes and blocked for 1 h at room temperature (RT) or overnight (O.N.) 4 °C with 5% powdered milk. The membrane was incubated with appropriate primary antibody either for 1 h at RT or O.N. at 4 °C. After washing, the membrane was incubated with the secondary antibody coupled with horseradish peroxidase for 1 h at RT. Band densitometry was done in ImageJ software (https://imagej.nih.gov/ij/download.html) (NIH) or in Image Lab 6.1 (https://www.bio-rad.com/en-ro/product/image-lab-software?ID=KRE6P5E8Z#fragment-6) software from Bio-Rad and normalized to the corresponding loading controls. The fold changes were calculated by dividing the KO value by the average WT value and were represented as mean ± SD

For extraction of insoluble fractions, the pellet was collected after 1% NP-40 extraction and 14,000 rpm centrifugation which was further resuspended in lysis buffer with 1% SDS and 50 mM DTT and boiled at 95 °C for 10 min.

For glycolytic treatments, approximately 10 μg total protein from cell lysate was used in reactions with either Endo H or PNGase F (New England Biolabs) according to a protocol described in the datasheet of the products.

For lysosomal and proteasomal inhibition, the cells were seeded in 12- or 6-well plates and were incubated with either 25 μM MG132 or 106 μM leupeptin and 14.5 μM pepstatin for 5 h. In other experiments, cells were treated with 100 nM bafilomycin A1 for 5 h.

For the treatment with cyclodextrin, the cells were seeded in a 6-well plate and were incubated for 48 h in medium containing 50 μM 2-hydroxypropyl-β-cyclodextrin.

Measurement of TYR activity in gel

TYR activity was measured by dopa-oxidase assay as follows: equal amounts of protein from MNT-WT and NPC1-KO cell lysates were separated by SDS-PAGE; the gel was incubated with L-DOPA in 0.1 M phosphate solution pH 6.8 and after 20 min was examined for a TYR band.

Immunoprecipitation

Harvested cells were lysed in 2% CHAPS buffer supplemented with a protease inhibitor cocktail for 30 min on ice and were cleared by centrifugation at 14,000*g* for 20 min. The lysates were incubated with anti-Pep7 antibody O.N. at 4 °C and further captured on protein A Sepharose (cat. 101041, Invitrogen-Life Technologies) for 2 h at 4 °C. After washing, the complexes were eluted with Laemmli buffer (LB: 50 mM Tris–HCl pH 6.8, 10% (w/v) glycerol, 2% (w/v) SDS, 0.004% bromophenol blue supplemented DTT) by boiling at 95 °C for 5 min. The eluted samples were handled for Western blotting.

Isolation of extracellular vesicles

The 48 h cell culture medium (or supernatant) was collected from subconfluent cell cultures. A centrifugation step at 300*g* for 10 min was performed first in order to remove dead cells and debris. The supernatant was centrifuged at 1200*g* for 20 min. The supernatant was transferred to a fresh tube and centrifuged at 110,000*g*, 4 °C for 2 h in a 70 Ti Beckman rotor. The pellet was washed in PBS, pH 7.4 and centrifuged again at 110,000*g*, 4 °C for 90 min in a 70 Ti rotor. Finally, the pellet was resuspended in a 1% Triton buffer and analyzed by Western blotting.

Subcellular fractionation

Subcellular fractionation of the organelles was conducted according to a protocol described in (46, 56). Briefly, cells were harvested and homogenized in a buffer containing 0.2 M sucrose and 10 mM Hepes and centrifuged at 1000*g*, 10 min at 4 °C. The supernatant was recovered and gently added to the sucrose gradient. It was further centrifuged at 100,000*g*, 1 h at 4 °C and 12 layers were recovered. LB was added to the fractions and was processed as for Western blotting. Sucrose gradient concentrations, from top to bottom: 1.0, 1.2, 1.4, 1.5, 1.6, 1.8, and 2.0 M, 4 ml each.

RNA isolation and real time qRT-PCR

Approximately 4 × 10^6 cells were seeded in a 6-well plate. After 48 h,cells were harvested in TRIzol reagent (Invitrogen) for total RNA isolation according to the manufacturer's specifications. The RNA concentration was determined by Nanodrop, and 50 ng RNA was further converted to complementary DNA and amplified in one step reaction using SensiFast Syber green kit. For the PCR amplification, TYR primers 5′-CTGGGATAGCGGATGCCTCTCAAAGC-3′ and 5′ -GCATGGTGAAGAAGGAAGATAGGATCGTTGG-3′. As housekeeping gene we used actin with the following primers 5′ -GTGATGGTGGGCATGGGTCAGAAGG-3′ and 5′ -GATGCCGTGCTCGATGGGGTACTTC-3′ were used. The reactions were performed using the Rotor-Gene 6000 instrument from Corbett Life Science, a Qiagen Company. The program for the amplification include following steps: initial reverse transcription at 42 °C for 10 min, polymerase activation at 95 °C for 2 min and cycling step (95 °C-5 s, 60 °C-5 s, 72 °C-5 s). RNA expression for TYR gene was normalized to actin as a reference gene.

GSLs extraction and analysis

GSLs were extracted from cell homogenates and analyzed by HPLC as described previously (57). Lipids were extracted in CHCl3:MeOH (1:2/V:V) O.N. at RT. The solution was centrifuged, the upper phase was mixed with PBS:CHCl3 (1:1) and centrifuged at 16,000*g*, 10 min, at RT. The lower phase was moved into a new tube and was dried down under nitrogen stream in a heating block. Further, it was resuspended in CHCl3/MeOH (1:3) and the upper phase was added. The C18 Isolute columns (100 mg, Biotage) were pre-equilibrated by adding 4 × 1 ml MeOH and 3 × 1 ml deionized water. The lipids were recovered on C18 Isolute columns and eluted with CHCl3:MeOH (98:2), CHCl3:MeOH (1:3), and MeOH. The column eluant was dried under a stream of nitrogen in

heating block and resuspended in ceramide glycanase buffer. The enzyme, CGase (50 μU, recombinant Endoglycoceramidase I, GenScript), was added and sample incubated O.N. at 37 °C. The released lipids were labeled with anthranilic acid. The labeling mix contains 30 mg/ml anthranilic acid and 45 mg/ml sodium cyanoborohydride. The samples were incubated with the labeling mix at 80 °C for 1 h were cooled at RT and acetonitrile (ACN):H20 (97:3) was added. Further, they were purified on Discover DPA-6S columns pre-equilibrated with 1 ml ACN, 2 × 1 ml water and 2 × 1 ml ACN. The columns were washed with ACN:H2O (95:5), and the samples were eluted in water. The eluent was loaded 60:140 sample: MeCN (v/v) for normal phase HPLC.

Cholesterol assay

Cholesterol was measured using the Amplex Red Cholesterol assay kit (Thermo Fisher Scientific), according to the manufacturer's instructions.

Immunofluorescence

The cells were fixed with 4% paraformaldehyde for 15 min, blocked, and permeabilized in PBS containing 1% bovine serum albumin and 0.1% saponin for 1 h and stained with primary antibodies O.N. at 4 °C in a wet chamber. The next day, the coverslips were washed and the corresponding secondary antibodies were added for 40 min at RT. Images were acquired using a Zeiss-LSM 700 (63×, 1.4 NA, oil) (Zeiss). The co-localization extent was measured using ImageJ, BIOP JACoP plugin and the thresholded Manders' coefficients were plotted (58). The mean fluorescence intensity of LAMP-2 was measured in ImageJ using region of interest for each cell and the mean gray value was plotted.

Statistical analysis

The data were processed using one-way, two-way ANOVA or *t* Student test with Prism6 (GraphPad software). Results with a *p* value of less than 0.05 were considered significant ($^{****}p < 0.0001$; $^{***}p < 0.001$; $^{**}p < 0.01$; $^{*}p < 0.05$) as indicated in the figure legends.

Sample preparation for LC-MS

MNT-WT and NPC1-KO cells were lysed in 1% NP40 buffer for 30 min on ice and subsequently centrifuged at 14,000*g*. Equal amounts of proteins, quantified using bicinchoninic acid assay, were separated by SDS-PAGE, were stained with Coomassie blue and further prepared for MS analysis as described in gel digestion protocols (34, 59, 60). Succinctly, the gel slices were washed with 40 mM ammonium bicarbonate and ACN. The disulfide bonds were reduced with DTT and cysteine sites were alkylated with iodoacetamide. The samples were digested in gel by trypsinization O.N. at 37 °C and the resulting peptides were subjected to multiple extractions with 5% formic acid (FA) and ACN. The eluted peptides were concentrated to dryness in a SpeedVac.

LC-MS/MS analysis

The samples were reconstituted in solvent A (0.06% FA and 2% ACN) and injected for nanoLC-MS/MS connected to an LTQ-Orbitrap Velos Pro instrument (Thermo Fisher Scientific). The loaded peptides were separated on a 15 cm Acclaim PepMap 100 C18 HPLC trap column using a 2 to 30% solvent B (0.06% FA and 80% ACN) and the eluted peptides were further analyzed using a LTQ-Orbitrap Velos Pro instrument (Thermo Fisher Scientific) as previously described (34).

All raw LC-MS/MS files were searched against the human version of the UniProt database using Andromeda algorithm included into MaxQuant computational proteomics platform. The settings included Trypsin/P as the used protease using maximum two missing cleavages, 10 ppm as mass accuracy for precursor ions, Cys carbomethylation as fixed modification and as variable modification were selected Met oxidation and N-terminus acetylation. Further, the results were filtered for 1% false discovery rate at peptide-spectrum match level with a peptide mass deviation of maximum 5 ppm.

Perseus software (19), version 2.0.6.0 (https://maxquant.net/perseus/) was applied for proteomic data analysis using label-free quantitation (LFQ) intensity. The data were filtered for identifications from the reversed database and proteins identified by site and the LFQ intensities were log2 transformed. Missing data were imputed from normal distribution using a width of 0.3 and a down shift of 1.8. For statistical analysis, a two-sample *t* test between NPC1-KO samples and control samples (MNT-WT) was applied (n = 3 biological replicates). Differentially expressed proteins were determined using a *p*-value cutoff less than 0.05. Heatmap of differentially expressed proteins was plotted using ComplexHeatmap R package. Principal component analysis plot was performed in Perseus 2.0.6.0 using log2 transformed LFQ intensities, considering the proteins that were identified in all samples.

Data availability

The authors confirm that the data supporting the findings of this study are available within the article [and/or] its supplementary materials. The mass spectrometry proteomics data have been deposited to the ProteomeXchange Consortium *via* the PRIDE partner repository with the dataset identifier: PXD042762.

Supporting information—This article contains supporting information.

Author contributions—A. A. R., I. V. M., I. P., C. V. A. M., L. E. S., and S. M. P. methodology; A. A. R., I. V. M., I. P., C. V. A. M., and L. E. S. investigation; A. A. R. and S. M. P. writing–original draft; A. A. R., F. M. P., and S. M. P. conceptualization; A. A. R., I. V. M., I. P., C. V. A. M., and L. E. S., formal analysis; I. V. M., I. P., and C. V. A. M. validation; N. P. and F. M. P. writing–review and editing; N. P., F. M. P., and S. M. P. supervision; F. M. P. and S. M. P. funding.

Funding and additional information—This work was funded by the Romanian Academy Project 1, 2019 to 2022 (to S. M. P., A. A. R., I. V. M., I. P., C. V. A. M., and L. E. S.), Horizon 2020–Marie

Skłodowska-Curie Research and Innovation Staff Exchange (RISE) (LysoMod) program, Grant Agreement no. 734825 (A. A. R., S. M. P., and F. M. P.). F. M. P. was supported by LysoMod, is a Wellcome Investigator in Science and a Wolfson Merit Award Holder.

Conflict of interest—The authors declare that they have no conflicts of interest with the contents of this article.

Abbreviations—The abbreviations used are: ACN, acetonitrile; ApoE, apolipoprotein; DCT, dopachrome-tautomerase; DOPA, 3,4 dihydroxy-L-phenylalanine; Endo H, endoglycosidase H; ER, endoplasmic reticulum; GlcCer, glucosylceramidase; GSL, glycosphingolipids; HMB, human melanoma black; LAMP, lysosome-associated membrane protein; LFQ, label-free quantitation; LRO, lysosome-related organelles; MITF, microphthalmia-associated transcription factor; MS, mass spectrometry; NPC, Niemann–Pick disease type C1; NPC1, Niemann–Pick type C1; O. N., overnight; PNGase F, peptide-N glycosidase F; RT, room temperature; TGN, *trans*-Golgi network; TYR, tyrosinase; TYRP, tyrosinase-related protein.

References

1. Gong, X., Qian, H., Zhou, X., Wu, J., Wan, T., Cao, P., *et al.* (2016) Structural insights into the niemann-Pick C1 (NPC1)-mediated cholesterol transfer and ebola infection. *Cell* **165**, 1467–1478
2. Evans, W. R. H., and Hendriksz, C. J. (2017) Niemann-Pick type C disease – the tip of the iceberg? a review of neuropsychiatric presentation, diagnosis and treatment. *BJpsych Bull.* **41**, 109–114
3. Wheeler, S., and Sillence, D. J. (2020) Niemann–Pick type C disease: cellular pathology and pharmacotherapy. *J. Neurochem.* **153**, 674–692
4. Li, X., Saha, P., Li, J., Blobel, G., and Pfeffer, S. R. (2016) Clues to the mechanism of cholesterol transfer from the structure of NPC1 middle lumenal domain bound to NPC2. *Proc. Natl. Acad. Sci. U. S. A.* **113**, 10079–10084
5. Höglinger, D., Burgoyne, T., Sanchez-Heras, E., Hartwig, P., Colaco, A., Newton, J., *et al.* (2019) NPC1 regulates ER contacts with endocytic organelles to mediate cholesterol egress. *Nat. Commun.* **10**, 4276
6. Pfeffer, S. R. (2019) NPC intracellular cholesterol transporter 1 (NPC1)-mediated cholesterol export from lysosomes. *J. Biol. Chem.* **294**, 1706–1709
7. Sitaram, A., and Marks, M. S. (2012) Mechanisms of protein delivery to melanosomes in pigment cells. *Physiology (Bethesda)* **27**, 85–99
8. Raposo, G., Marks, M. S., and Cutler, D. F. (2007) Lysosome-related organelles: driving post-Golgi compartments into specialisation. *Curr. Opin. Cell Biol.* **19**, 394–401
9. Buitenkamp, T. D., Izraeli, S., Zimmermann, M., Forestier, E., Heerema, N. A., van den Heuvel-Eibrink, M. M., *et al.* (2014) Acute lymphoblastic leukemia in children with Down syndrome: a retrospective analysis from the Ponte di Legno study group. *Blood* **123**, 70–77
10. Chen, O. C. W., Colaco, A., Davis, L. C., Kiskin, F. N., Farhat, N. Y., Speak, A. O., *et al.* (2020) Defective platelet function in Niemann-Pick disease type C1. *JIMD Rep.* **56**, 46–57
11. Le, L., Sirés-Campos, J., Raposo, G., Delevoye, C., and Marks, M. S. (2021) Melanosome biogenesis in the pigmentation of mammalian skin. *Integr. Comp. Biol.* **61**, 1517–1545
12. Raposo, G., and Marks, M. S. (2007) Melanosomes — dark organelles enlighten endosomal membrane transport. *Nat. Rev. Mol. Cell Biol.* **8**, 786–797
13. Bissig, C., Rochin, L., and van Niel, G. (2016) PMEL amyloid fibril formation: the bright steps of pigmentation. *Int. J. Mol. Sci.* **17**, 1438
14. Petrescu, S. M., Branza-Nichita, N., Negroiu, G., Petrescu, A. J., and Dwek, R. A. (2000) Tyrosinase and glycoprotein folding: roles of chaperones that recognize glycans. *Biochemistry* **39**, 5229–5237
15. Ando, H., Ichihashi, M., and Hearing, V. (2009) Role of the ubiquitin proteasome system in regulating skin pigmentation. *Int. J. Mol. Sci.* **10**, 4428–4434
16. Yamaguchi, Y., and Hearing, V. J. (2014) Melanocytes and their diseases. *Cold Spring Harb. Perspect. Med.* **4**, a017046
17. Branza-Nichita, N., Petrescu, A. J., Dwek, R. A., Wormald, M. R., Platt, F. M., and Petrescu, S. M. (1999) Tyrosinase folding and copper loading *in Vivo*: a crucial role for calnexin and α-glucosidase II. *Biochem. Biophys. Res. Commun.* **261**, 720–725
18. Popescu, C. I., Mares, A., Zdrentu, L., Zitzmann, N., Dwek, R. A., and Petrescu, S. M. (2006) Productive folding of tyrosinase ectodomain is controlled by the transmembrane anchor. *J. Biol. Chem.* **281**, 21682–21689
19. Petrescu, S. M., Petrescu, A. J., Titu, H. N., Dwek, R. A., and Platt, F. M. (1997) Inhibition of N-glycan processing in B16 melanoma cells results in inactivation of tyrosinase but does not prevent its transport to the melanosome. *J. Biol. Chem.* **272**, 15796–15803
20. Marin, M. B., Ghenea, S., Spiridon, L. N., Chiritoiu, G. N., Petrescu, A. J., and Petrescu, S. M. (2012) Tyrosinase degradation is prevented when EDEM1 lacks the intrinsically disordered region. *PLoS One* **7**, e42998
21. Petrescu, S. M., Popescu, C. I., Petrescu, A. J., and Dwek, R. A. (2003) The glycosylation of tyrosinase in melanoma cells and the effect on antigen presentation. *Adv. Exp. Med. Biol.* **535**, 257–269
22. Watabe, H., Valencia, J. C., Yasumoto, K. I., Kushimoto, T., Ando, H., Muller, J., *et al.* (2004) Regulation of tyrosinase processing and trafficking by organellar pH and by proteasome activity. *J. Biol. Chem.* **279**, 7971–7981
23. Wang, N., and Hebert, D. N. (2006) Tyrosinase maturation through the mammalian secretory pathway: bringing color to life. *Pigment Cell Res.* **19**, 3–18
24. Vruchte, D. T., Lloyd-Evans, E., Veldman, R. J., Neville, D. C. A., Dwek, R. A., Platt, F. M., *et al.* (2004) Accumulation of glycosphingolipids in niemann-Pick C disease disrupts endosomal transport. *J. Biol. Chem.* **279**, 26167–26175
25. Kaya, E., Smith, D. A., Smith, C., Morris, L., Bremova-Ertl, T., Cortina-Borja, M., *et al.* (2021) Acetyl-leucine slows disease progression in lysosomal storage disorders. *Brain Commun.* **3**, fcaa148
26. Sprong, H., Degroote, S., Claessens, T., van Drunen, J., Oorschot, V., Westerink, B. H. C., *et al.* (2001) Glycosphingolipids are required for sorting melanosomal proteins in the Golgi complex. *J. Cell Biol.* **155**, 369–380
27. Smit, N. P. M., Aerts, J. M. F. G., Groener, J. E. M., and Pavel, S. (2003) SP-18 Inhibition of glycolipid synthesis reduces melanin production in cultured human melanocytes. *Pigment Cell Res.* **16**, 585
28. Groux-Degroote, S., van Dijk, S. M., Wolthoorn, J., Neumann, S., Theos, A. C., De Mazière, A. M., *et al.* (2008) Glycolipid-dependent sorting of melanosomal from lysosomal membrane proteins by lumenal determinants. *Traffic* **9**, 951–963
29. Colaco, A., Kaya, E., Adriaenssens, E., Davis, L. C., Zampieri, S., Fernández-Suárez, M. E., *et al.* (2020) Mechanistic convergence and shared therapeutic targets in Niemann-Pick disease. *J. Inherit. Metab. Dis.* **43**, 574–585
30. Militaru, I. V., Rus, A. A., Munteanu, C. V. A., Manica, G., and Petrescu, S. M. (2023) New panel of biomarkers to discriminate between amelanotic and melanotic metastatic melanoma. *Front. Oncol.* **12**, 1061832
31. Kawakami, A., and Fisher, D. E. (2017) The master role of microphthalmia-associated transcription factor in melanocyte and melanoma biology. *Lab. Invest.* **97**, 649–656
32. Schallreuter, K. U., Hasse, S., Rokos, H., Chavan, B., Shalbaf, M., Spencer, J. D., *et al.* (2009) Cholesterol regulates melanogenesis in human epidermal melanocytes and melanoma cells. *Exp. Dermatol.* **18**, 680–688
33. Tanaka, Y., Yamada, Y., Ishitsuka, Y., Matsuo, M., Shiraishi, K., Wada, K., *et al.* (2015) Efficacy of 2-Hydroxypropyl-β-cyclodextrin in niemann–Pick disease type C model mice and its pharmacokinetic analysis in a patient with the disease. *Biol. Pharm. Bull.* **38**, 844–851
34. Chiritoiu, G. N., Jandus, C., Munteanu, C. V. A., Ghenea, S., Gannon, P. O., Romero, P., *et al.* (2016) Epitope located *N* -glycans impair the MHC-I epitope generation and presentation: proteomics and 2-DE. *Electrophoresis* **37**, 1448–1460

35. Cawley, N. X., Sojka, C., Cougnoux, A., Lyons, A. T., Nicoli, E., Wassif, C. A., *et al.* (2020) Abnormal LAMP1 glycosylation may play a role in Niemann-Pick disease, type C pathology. *PLoS One* **15**, e0227829
36. van Niel, G., Bergam, P., Di Cicco, A., Hurbain, I., Lo Cicero, A., Dingli, F., *et al.* (2015) Apolipoprotein E regulates amyloid formation within endosomes of pigment cells. *Cell Rep.* **13**, 43–51
37. Tang, B. L. (2019) Syntaxin 16's newly deciphered roles in autophagy. *Cells* **8**, 1655
38. Graham, S. C., Wartosch, L., Gray, S. R., Scourfield, E. J., Deane, J. E., Luzio, J. P., *et al.* (2013) Structural basis of Vps33A recruitment to the human HOPS complex by Vps16. *Proc. Natl. Acad. Sci. U. S. A.* **110**, 13345–13350
39. Mauvezin, C., and Neufeld, T. P. (2015) Bafilomycin A1 disrupts autophagic flux by inhibiting both V-ATPase-dependent acidification and Ca-P60A/SERCA-dependent autophagosome-lysosome fusion. *Autophagy* **11**, 1437–1438
40. Phuyal, S., Hessvik, N. P., Skotland, T., Sandvig, K., and Llorente, A. (2014) Regulation of exosome release by glycosphingolipids and flotillins. *FEBS J.* **281**, 2214–2227
41. Seguin, S. J., Morelli, F. F., Vinet, J., Amore, D., De Biasi, S., Poletti, A., *et al.* (2014) Inhibition of autophagy, lysosome and VCP function impairs stress granule assembly. *Cell Death Differ.* **21**, 1838–1851
42. Kao, S. H., Wang, W. L., Chen, C. Y., Chang, Y. L., Wu, Y. Y., Wang, Y. T., *et al.* (2015) Analysis of protein stability by the cycloheximide chase assay. *Bio Protoc.* **5**, e1374
43. Manders, E. M. M., Verbeek, F. J., and Aten, J. A. (1993) Measurement of co-localization of objects in dual-colour confocal images. *J. Microsc.* **169**, 375–382
44. Wasmeier, C., Romao, M., Plowright, L., Bennett, D. C., Raposo, G., and Seabra, M. C. (2006) Rab38 and Rab32 control post-Golgi trafficking of melanogenic enzymes. *J. Cell Biol.* **175**, 271–281
45. Graham, M., Tzika, A. C., Mitchell, S. M., Liu, X., and Leonhardt, R. M. (2019) Repeat domain-associated O-glycans govern PMEL fibrillar sheet architecture. *Sci. Rep.* **9**, 6101
46. Kushimoto, T., Basrur, V., Valencia, J., Matsunaga, J., Vieira, W. D., Ferrans, V. J., *et al.* (2001) A model for melanosome biogenesis based on the purification and analysis of early melanosomes. *Proc. Natl. Acad. Sci. U. S. A.* **98**, 10698–10703
47. Claudepierre, T., Paques, M., Simonutti, M., Buard, I., Sahel, J., Maue, R. A., *et al.* (2010) Lack of Niemann–Pick type C1 induces age-related degeneration in the mouse retina. *Mol. Cell. Neurosci.* **43**, 164–176
48. Schallreuter, K. U., Hasse, S., Rokos, H., Chavan, B., Shalbaf, M., Spencer, J. D., *et al.* (2009) Cholesterol regulates melanogenesis in human epidermal melanocytes and melanoma cells. *Exp. Dermatol.* **18**, 680–688
49. Bu, J., Ma, P. C., Chen, Z. Q., Zhou, W. Q., Fu, Y. J., Li, L. J., *et al.* (2008) Inhibition of MITF and tyrosinase by Paeonol-stimulated JNK/SAPK to reduction of phosphorylated CREB. *Am. J. Chin. Med.* **36**, 245–263
50. Yasumoto, K., Yokoyama, K., Shibata, K., Tomita, Y., and Shibahara, S. (1994) Microphthalmia-associated transcription factor as a regulator for melanocyte-specific transcription of the human tyrosinase gene. *Mol. Cell. Biol.* **14**, 8058–8070
51. Yasumoto, K. I., Yokoyama, K., Takahashi, K., Tomita, Y., and Shibahara, S. (1997) Functional analysis of microphthalmia-associated transcription factor in pigment cell-specific transcription of the human tyrosinase family genes. *J. Biol. Chem.* **272**, 503–509
52. Scott, C., Higgins, M. E., Davies, J. P., and Ioannou, Y. A. (2004) Targeting of NPC1 to late endosomes involves multiple signals, including one residing within the putative sterol-sensing domain. *J. Biol. Chem.* **279**, 48214–48223
53. Storch, S., Pohl, S., and Braulke, T. (2004) A dileucine motif and a cluster of acidic amino acids in the second cytoplasmic domain of the batten disease-related CLN3 protein are required for efficient lysosomal targeting. *J. Biol. Chem.* **279**, 53625–53634
54. Theos, A. C., Tenza, D., Martina, J. A., Hurbain, I., Peden, A. A., Sviderskaya, E. V., *et al.* (2005) Functions of adaptor protein (AP)-3 and AP-1 in tyrosinase sorting from endosomes to melanosomes. *Mol. Biol. Cell* **16**, 5356–5372
55. Valmori, D., Marañón Lizana, C., Liénard, D., Rimoldi, D., Jongeneel, V., Cerottini, J. C., *et al.* (1997) Enhanced generation of specific tumor-reactive CTL in vitro by Melan-A/Mart-1 immunodominant peptide analogs. *Immunol. Lett.* **56**, 223–224
56. Watabe, H., Kushimoto, T., Valencia, J. C., and Hearing, V. J. (2005) Isolation of melanosomes. In: Bonifacino, J. S., Dasso, M., Harford, J. B., Lippincott-Schwartz, J., Yamada, K. M., eds. *Current Protocols in Cell Biology*, John Wiley & Sons, Inc, Hoboken, NJ
57. Neville, D. C. A., Coquard, V., Priestman, D. A., te Vruchte, D. J. M., Sillence, D. J., Dwek, R. A., *et al.* (2004) Analysis of fluorescently labeled glycosphingolipid-derived oligosaccharides following ceramide glycanase digestion and anthranilic acid labeling. *Anal. Biochem.* **331**, 275–282
58. Dunn, K. W., Kamocka, M. M., and McDonald, J. H. (2011) A practical guide to evaluating colocalization in biological microscopy. *Am. J. Physiol. Cell Physiol.* **300**, C723–C742
59. Shevchenko, A., Tomas, H., Havli, J., Olsen, J. V., and Mann, M. (2006) In-gel digestion for mass spectrometric characterization of proteins and proteomes. *Nat. Protoc.* **1**, 2856–2860
60. Munteanu, C. V. A., Chiriţoiu, G. N., Petrescu, A. J., and Petrescu Ştefana, M. (2019) Profiling optimal conditions for capturing EDEM proteins complexes in melanoma using mass spectrometry. *Adv. Exp. Med. Biol.* **1140**, 155–167